# 2. GEOCHEMICAL VARIATIONS IN A SINGLE BASALTIC FLOW AT 9°30′N ON THE EAST PACIFIC RISE[1]

## Karen S. Harpp[2]

### ABSTRACT

Basalts collected during Ocean Drilling Program Leg 142 from a single site at 9°30′N on the East Pacific Rise have been analyzed for Sr, Nd, and Pb isotope ratios by thermal ionization mass spectrometry, and trace element concentrations (rare earth elements, Ba, Y, Zr, Nb, Hf, and Ta) by inductively coupled-plasma mass spectrometry. Samples exhibit a small range in geochemical variations. Mean isotopic values for the data set are $0.702484 \pm 0.000011$ ($1\sigma$) for $^{87}Sr/^{86}Sr$, $9.70 \pm 0.27$ ($1\sigma$) for $\varepsilon_{Nd}$, $18.300 \pm 0.025$ ($1\sigma$), $15.477 \pm 0.016$ ($1\sigma$), and $37.705 \pm 0.062$ ($1\sigma$) for $^{206}Pb/^{204}Pb$, $^{207}Pb/^{204}Pb$, and $^{208}Pb/^{204}Pb$, respectively. Trace element compositions are also typical of normal-type mid-ocean ridge basalt. Detailed statistical analysis indicates that the lavas are indistinguishable in terms of their isotopic ratios, Nb, Ta, Sr, Ni, Cu, and Zn concentrations, and most major oxide contents. Samples fall into two distinct units based on the concentrations of mostly incompatible elements, including the rare earth elements, Ba, Y, Zr, and Hf.

The relationship between the units cannot be explained by shallow-level phenomena including fractional crystallization or crystal settling but must have originated below the magma chamber, which is consistent with other Leg 142 studies (Brophy and Allan, this volume; Brophy, this volume). Samples are derived from two or more similar but distinct parental melts. The parental melts share the same mantle source, but evolved via different melt generation paths. The precise temporal relationship between Units 1 and 2 cannot be determined owing to the lack of stratigraphic control during drilling. Interunit geochemical variations may represent two (or more) eruptive events, or heterogeneity within a single flow. In either case, this information is useful in evaluating geochemical results from axial studies, particularly from the immediate 9°–10°N ridge area.

At a single site on the East Pacific Rise, variations in trace element concentrations are accompanied by isotopic homogeneity, suggesting that geochemical characteristics of and processes within the underlying mantle are the major factors controlling compositional variation at mid-ocean ridges, not shallow magma chamber processes. Large-scale phenomena such as mantle convection may be primarily responsible for the degree of isotopic heterogeneity at mid-ocean ridges, while complex mantle melting processes control trace element characteristics.

## INTRODUCTION

Ocean Drilling Program (ODP) Leg 142 was a test of the newly-developed diamond coring system at the East Pacific Rise (EPR), a bare rock site known for some of the most hostile drilling conditions in the world. Despite formidable engineering difficulties, shipboard engineers successfully recovered basalt samples from up to 15 m below the ridge axis (i.e., seafloor; mbsf). Based on X-ray fluorescence (XRF) analyses, thin section descriptions, and depths of recovery below seafloor, the Shipboard Scientific Party concluded the material represents two distinct lithologic units, each of which may have been emplaced by single eruptive events (Shipboard Scientific Party, 1993b).

Analysis of the Leg 142 samples permits testing of an assumption fundamental to geochemical ridge studies, namely that trace element concentrations and in particular isotopic signatures are identical within individual eruptive events. Two questions are raised by these results: are the two units geochemically distinct and is each unit geochemically homogeneous? Both questions are important in the context of detailed along-axis ridge studies. The answers will help determine whether the degree of geochemical variation detected along short spreading-center segments is meaningful in terms of mantle processes. That is, do isotope ratios and trace element concentrations vary within a lava flow or eruptive event to an analytically detectable degree or are they identical within analytical limits? Does the present level of analytical precision surpass the extent of homogenization that nature can produce?

This study involves a representative subset of the Leg 142 recovery, a total of 29 samples consisting of 4 glassy and 11 coarse-grained basalt fragments as well as 14 samples in powdered form. The latter were analyzed by XRF during shipboard studies. Strontium, neodymium, and lead isotope ratios were determined for selected samples using thermal ionization mass spectrometry (TIMS). Concentrations of the lanthanide rare earth elements (REEs), Ba, Y, Zr, Nb, Hf, and Ta, were measured by inductively coupled plasma-mass spectrometry (ICP-MS). Statistical analysis of these results indicate that the Leg 142 samples are isotopically indistinguishable but can be divided into two groups based on their elemental concentrations, confirming the conclusions of the Shipboard Scientific Party (1993b) that the recovery represents material from two distinct lithologic units. Geochemical results indicate that the two units originated from distinct parental melts and experienced a complex series of in situ fractionation processes prior to injection into the magma chamber. In the melt lens, the diverse liquid compositions were subjected to partial homogenization during localized convection before eruption.

## SAMPLE DESCRIPTIONS AND PROCESSING

### Drill Site

Site 864 is located on the floor of the EPR axial summit caldera (ASC) at 9°30.85′N, 104°14.66′W, at 2581 m depth. The base of the

**Table 1. ICP-MS standard values.**

| | | Ba | La | Ce | Pr | Nd | Sm | Eu | Gd | Tb | Dy | Ho | Er | Tm | Yb | Lu |
|---|---|---|---|---|---|---|---|---|---|---|---|---|---|---|---|---|
| BIR-1 | m | 6.6 | 0.65 | 1.89 | 0.39 | 2.39 | 1.10 | 0.49 | 1.91 | 0.38 | 2.52 | 0.58 | 1.63 | 0.26 | 1.63 | 0.26 |
| | $s_a$ | 0.3 | 0.06 | 0.08 | 0.02 | 0.09 | 0.05 | 0.02 | 0.10 | 0.02 | 0.10 | 0.03 | 0.07 | 0.02 | 0.07 | 0.02 |
| | $n$ | 45 | 46 | 46 | 46 | 46 | 46 | 46 | 46 | 46 | 46 | 46 | 46 | 46 | 46 | 46 |
| DNC-1 | m | 105 | 3.74 | 8.19 | 1.13 | 5.04 | 1.45 | 0.60 | 2.16 | 0.42 | 2.79 | 0.65 | 1.87 | 0.30 | 1.97 | 0.32 |
| | $s_a$ | 3.1 | 0.12 | 0.33 | 0.04 | 0.17 | 0.06 | 0.02 | 0.10 | 0.02 | 0.10 | 0.03 | 0.07 | 0.01 | 0.09 | 0.01 |
| | $n$ | 56 | 58 | 58 | 58 | 58 | 58 | 58 | 58 | 58 | 58 | 58 | 58 | 58 | 58 | 58 |
| W2 | m | 172 | 10.69 | 23.4 | 3.07 | 13.20 | 3.31 | 1.10 | 3.91 | 0.68 | 3.92 | 0.81 | 2.18 | 0.33 | 2.08 | 0.33 |
| | $s_a$ | 5.0 | 0.30 | 0.8 | 0.11 | 0.40 | 0.12 | 0.04 | 0.11 | 0.02 | 0.10 | 0.03 | 0.06 | 0.01 | 0.08 | 0.02 |
| | $n$ | 69 | 75 | 75 | 75 | 75 | 75 | 75 | 75 | 75 | 75 | 75 | 75 | 75 | 75 | 75 |
| BHVO-1 | m | 130 | 15.29 | 37.3 | 5.37 | 24.64 | 6.06 | 1.98 | 6.48 | 1.04 | 5.36 | 1.00 | 2.44 | 0.34 | 2.00 | 0.29 |
| | $s_a$ | 4.4 | 0.33 | 0.7 | 0.09 | 0.41 | 0.12 | 0.04 | 0.13 | 0.02 | 0.14 | 0.03 | 0.08 | 0.02 | 0.08 | 0.02 |
| | $n$ | 53 | 54 | 54 | 54 | 54 | 54 | 54 | 54 | 54 | 54 | 54 | 54 | 54 | 54 | 54 |

Notes: Values are in ppm. m = mean; $s_a$ = analytical standard deviation; $n$ = number of analyses.

ASC at the site consists of a flat-to-ropey massive basalt flow known as the ODP Flow, 3.5 m thick and 60 m wide (Shipboard Scientific and Engineering Parties, 1993). Three holes were attempted: 864A, 864B, and 864C. Holes 864A and 864B were cased to 13.3 and 7.1 mbsf, respectively. Material was recovered from drill bits, core barrels, and junk baskets primarily from Hole 864A, with a small contribution from Hole 864B. During drilling and hole-cleaning operations at Holes 864A and 864B, two lithologies were recovered: abundant, primarily glassy fragments from thin sheet or lobate flows underlying the massive ODP Flow at the surface, and more massive, coarser-grained material presumably representing the interior of a thick flow. Material was assigned to two lithologic units by the Shipboard Scientists based on (1) depth of recovery; (2) petrographic descriptions; and (3) geochemical differences determined by XRF analyses.

Unit 1 consists of the uppermost 2- to 3-m-thick massive flow underlain by a few meters of glassy lobate or sheet flows (Cores 142-864A-1M and 142-864B-2W) (Shipboard Scientific Party, 1993b). The thickness of Unit 1 must be less than 6.6 m, according to drilling depths. Based on the homogeneity of petrographic and geochemical observations, the Shipboard Scientific Party (1993b) concluded that all Unit 1 material was probably emplaced during a single eruptive event.

The lowermost massive unit (Cores 142-864A-3Z through -5Z) is designated as Unit 2. This lithology consists of a thick, jointed lava flow or possibly a dike of undetermined thickness recovered from a drilling interval from 11.8 to 15.0 mbsf and is separated from Unit 1 by an interval in which no material was recovered (Shipboard Scientific Party, 1993b). Without better stratigraphic control it is not possible to distinguish whether Unit 2 samples originated with Unit 1 material in a single event or as a separate, earlier eruption.

Unit 1 differs from Unit 2 in a number of subtle ways. Unit 2 contains up to 2 volume percent phenocrysts whereas Unit 1 is only sparsely phyric with less than 1% phenocrysts (Shipboard Scientific Party, 1993b). Unit 1 phenocrysts consist largely of plagioclase, whereas some clinopyroxene and rare olivine crystals are found in Unit 2 samples in addition to the predominant plagioclase. The plagioclase phenocrysts observed in Unit 2 are larger, more tabular, and slightly resorbed. Based on initial shipboard geochemical results including XRF and carbon, hydrogen, and oxygen analysis, both units exhibit somewhat evolved normal-type mid-ocean ridge basalt compositions (N-MORB). Relative to Unit 1, however, Unit 2 contains slightly higher concentrations of $Na_2O$, $TiO_2$, Y, and Zr, and lower concentrations of $Al_2O_3$, CaO, and Cr (Shipboard Scientific Party, 1993b).

## Shipboard Processing

Junk basket samples (Sections 142-864A-1M-2,-3,-5, and -6) were rinsed with deionized water to remove contaminants including drilling fluids, paint flakes, and metal drill bit fragments. The samples were passed through sieves and divided into three size fractions, <1 mm, 1 to 5 mm, and 5 mm to 5 cm. Remaining pieces of paint or metal were removed by hand as much as possible from the coarsest sample fractions. The material was then ultrasonically treated in deionized water for several hours, with a change of liquid and a thorough rinse approximately every hour. The next stage of the cleaning process involved repeated rinses in acetone followed by methanol. Finally, samples were laid out to dry under a heat lamp. Only the largest-sized fractions were placed in the core jackets and used for further study. Solid samples consisting of larger single crystalline pieces from the drill bit and wash cores were not passed through this cleaning process.

Material collected from the junk baskets did not fit easily into the ODP classification scheme. Normally, samples are numbered according to their recovery depth below the seafloor. This could not be done for the fragments, because the only control available was the total hole depth at the time of retrieval. The labeled centimeter intervals within the cores do not represent a measurable depth in the hole. Instead, they are an indication of how much space that particular selection of material occupies in the core jackets. Samples from each junk basket were sorted according to material type, whether a sample was a large or small glass fragment, a coarse- or fine-grained crystalline piece, or if there were any visible alteration products. As a result, groupings at the interval level are somewhat arbitrary in the sense that samples were sorted based on visual criteria, prior to any geochemical or geophysical studies. In other words, basaltic fragments that might differ geochemically would be mixed together in a single core jacket compartment if they were visually indistinguishable. Shipboard powders consist of randomly-chosen fragments from each interval. Several single basalt pieces from individual intervals have been analyzed to address the potential difficulties inherent in this necessary but somewhat unconventional sample organization (see "Results" section below).

Powders were produced aboard *JOIDES Resolution* during Leg 142 by crushing in a Spex 8510 shatterbox with an alumina ceramic barrel. Shipboard tests using different barrels suggest no significant contamination of any element measured by XRF for the different grinding materials (Shipboard Scientific Party, 1993a). Although all powders were analyzed for trace element concentrations, in only a few cases were ground samples processed for Pb isotopes owing to fear of contamination during cleaning and grinding.

## ANALYTICAL PROCEDURES

### Elemental Concentrations

Samples were crushed using an iron Platner mortar and pestle and ultrasonically cleaned in quartz-distilled water for 15 min. Individual glass pieces (100–200 mg) or 100–200-mg chips from the interior of crystalline samples were selected for TIMS and ICP-MS analysis. All further handling and chemical procedures were conducted in a class

**Table 1 (continued).**

| Y | Zr | Nb | Hf | Ta |
|---|----|----|----|----|
| 17.1 | 15.5 | 0.58 | 0.59 | 0.04 |
| 0.4 | 0.5 | 0.03 | 0.04 | 0.01 |
| 22 | 22 | 22 | 26 | 26 |
| 19.6 | 39.4 | 1.65 | 1.04 | 0.09 |
| 0.6 | 1.6 | 0.11 | 0.05 | 0.01 |
| 26 | 26 | 26 | 19 | 19 |
| 24.4 | 97.9 | 7.90 | 2.55 | 0.50 |
| 0.8 | 3.2 | 0.35 | 0.11 | 0.02 |
| 38 | 29 | 38 | 24 | 24 |
| 29.2 | 183 | 19.74 | 4.61 | 1.23 |
| 0.4 | 2.0 | 0.30 | 0.14 | 0.04 |
| 46 | 46 | 46 | 35 | 35 |

1000 clean room. All reagents used in the following procedures were prepurified, according to the procedures described in Harpp (1994).

Concentrations of the rare earth elements, Ba, Y, Zr, Nb, Ta and Hf, were determined on a VG Fisons Plasmaquad PQ2+ ICP-MS. Trace element concentrations were measured using a nonlinear drift correction procedure and external calibration against matrix-matched standards as described by Cheatham et al. (1993). Results from replicate analyses of standard solutions are listed in Table 1. Isobaric interferences on Gd isotopes by oxides of Nd were corrected by subtracting 1%–5% of the Nd concentration from the initial Gd value, as dictated by the run conditions.

Where only the rare earth element concentrations were determined, approximately 0.25 g of material was dissolved following the $HClO_4/HNO_3$ dissolution procedure outlined in Cheatham et al. (1993). Samples for which the high field strength elements (Zr, Nb, Hf, and Ta) were measured in addition to the REEs were digested using the $HF/HNO_3$ dissolution procedure described in Harpp (1994). This latter method results in higher levels of fluoride ions in the final solution compared to the $HClO_4/HNO_3$ dissolution process. Increased fluoride ion concentration inhibits adsorption of Zr, Nb, Hf and Ta to the container walls. In addition, isobaric interferences involving the calcium perchlorate ion $CaClO_4^+$ primarily at mass [139]La as well as lesser interferences at higher odd masses ([141]Pr, [143]Nd, etc.) are avoided with the switch to the $HF/HNO_3$ dissolution technique (Longerich, 1993). The final solutions were diluted to 1/1000th the concentration of the original sample.

For comparison purposes, concentrations of Y, Zr, and Nb for equivalent powdered samples determined by ICP-MS at Cornell and by XRF aboard *JOIDES Resolution* are plotted against each other in Figure 1 (Shipboard Scientific Party, 1993b). Zr concentrations agree closely for both techniques, differing by an average of less than 2%, or ~2 ppm. Results for Y are consistently higher by ICP-MS than XRF, with an average difference of ~7%, equivalent to ~3 ppm. XRF and ICP-MS Nb concentrations deviate less systematically. They differ in their apparent precision; the ICP-MS values span only 0.2 ppm, whereas XRF concentrations for the same set of samples cover a range of almost 1 ppm. Despite similar reported analytical uncertainties for ICP-MS and XRF, ICP-MS appears to be more precise (Shipboard Scientific Party, 1993a). Replicate analyses of the standard material BHVO-1 were performed using both ICP-MS and shipboard XRF. ICP-MS results for Y, Zr, and Nb correspond closely to concentrations determined by high-precision isotope dilution-spark source mass spectrometry (ID-SSMS) (Jochum et al., 1990), differing by less than 0.9%. XRF means for BHVO-1 are more than 6% and 10% lower than the ID-SSMS values for Nb and Y, respectively; XRF and isotope dilution results correspond exactly for Zr. Based on the standard results, ICP-MS techniques are generally more accurate and precise than XRF for the determination of Y and Nb abundances and comparable for Zr analysis at the low concentration levels typical of N-MORB.
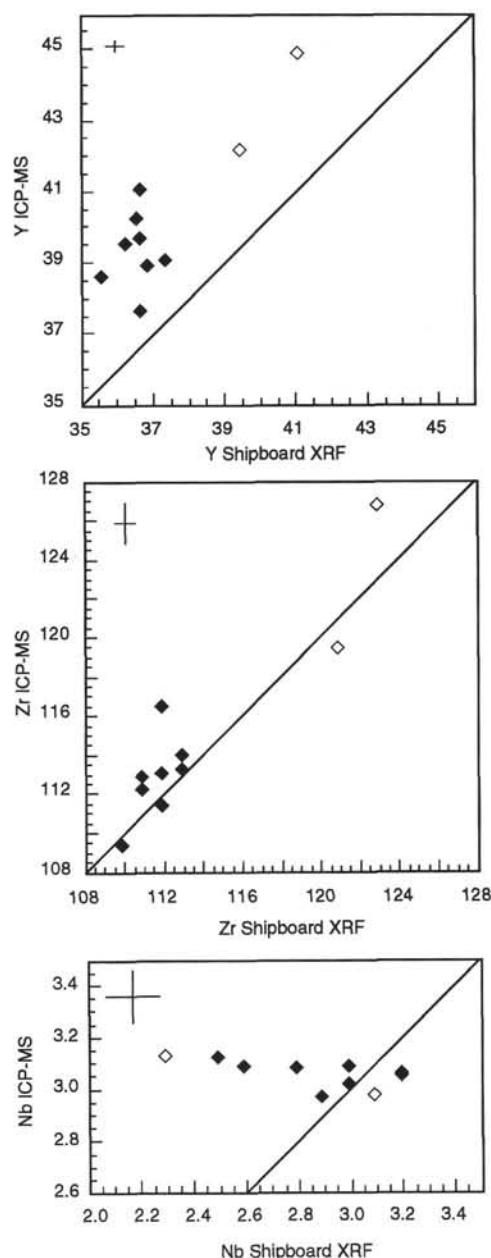


Figure 1. Comparison of ICP-MS with shipboard XRF analyses of Y, Zr, and Nb concentrations for selected Leg 142 powdered samples. Diagonal lines have slopes of one. Solid diamonds = Unit 1 samples; open diamonds = Unit 2 samples. Values are in ppm. Error bars represent one standard deviation analytical precision.

## Isotope Ratios

Prior to separation, approximately 250–300 mg of sample was leached for varying times (see Table 2 and further discussion) with HCl in covered containers to remove possible contamination induced by exposure to seawater, hydrothermal alteration, or drilling and handling. Detailed descriptions of the chemical separation procedures are listed in Harpp (1994). Strontium and REE splits were separated on a cation exchange column (BioRad AG50W-×12 resin, e.g., White and Patchett, 1984; Harpp, 1994). Neodymium was isolated according to the di-2-ethylhexyl orthophosphoric acid ion exchange technique (e.g., White and Patchett, 1984). Samples destined for Pb

**Table 2. Results of leaching, multiple-analysis, and sample-type isotope tests.**

| Core, section, interval (cm) | Sample type | $^{87}Sr/^{86}Sr$ | Leach strength | Minutes leached |
|---|---|---|---|---|
| Leaching experiments 142-864A- | | | | |
| 1M-3, 55–85 | Powder | 0.702505 | none | 0 |
| 1M-3, 55–85 | Powder | 0.702483 | 6M | 30 |
| 1M-6, 0–75 | Powder | 0.702499 | 2M | 15 |
| 1M-6, 0–75 | Powder | 0.702555 | 6M | 30 |
| 1M-6, 0–75 | Glass | 0.702471 | 2M | 30 |
| 1M-6, 0–75 | Glass | 0.702500 | 6M | 30 |
| 1M-3, 0–35 | Glass | 0.702468 | 2M | 15 |
| 1M-3, 0–35 | Glass | 0.702477 | 2M | 30 |
| 1M-3, 0–35 | Glass | 0.702505 | 6M | 30 |
| 142-864B- | | | | |
| 2W-1, 0–4 | Crystalline | 0.702478 | 2M | 15 |
| 2W-1, 0–4 | Crystalline | 0.702504 | 6M | 30 |
| 142-864A- | | | | |
| 4Z-1, 9–15 | Crystalline | 0.702490 | 2M | 15 |
| 4Z-1, 9–15 | Crystalline | 0.702479 | 6M | 30 |
| 5Z-1, 24–30 | Powder | 0.702562 | none | 0 |
| 5Z-1, 24–30 | Powder | 0.702477 | 6M | 30 |

| Core, section, interval (cm) | Sample type | $^{87}Sr/^{86}Sr$ | $\varepsilon_{Nd}$ |
|---|---|---|---|
| Multiple-analysis experiments 142-864A- | | | |
| 1M-6, 0–75 | Single glass piece | 0.702486 | 9.41 |
| 1M-6, 0–75 | Single glass piece | 0.702489 | 9.47 |
| 1M-6, 0–75 | Single glass piece | 0.702481 | 9.63 |
| 1M-6, 0–75 | Single glass piece | 0.702472 | |
| Sample-type experiments 142-864A- | | | |
| 1M-3, 55–85 | Powder | 0.702483 | |
| 1M-3, 54–84 | Crystalline | 0.702494 | 9.48 |
| 1M-3, 54–84 | Crystalline | | 9.33 |
| 1M-5, 0–100 | Powder | 0.702485 | |
| 1M-5, 0–100 | Glass* | 0.702473 | 9.21 |
| 1M-5, 0–100 | Crystalline | 0.702505 | 9.91 |
| 1M-6, 75–135 | Crystalline portion | 0.702489 | 9.98 |
| 1M-6, 75–135 | Glass portion | 0.702477 | |

Notes: Leaches were performed with HCl. * = small fragments.

**Table 3. Isotopic standard values.**

| | $^{87}Sr/^{86}Sr$ | $^{143}Nd/^{144}Nd$ | $^{143}Nd/^{144}Nd$ | $^{206}Pb/^{204}Pb$ | $^{207}Pb/^{204}Pb$ | $^{208}Pb/^{204}Pb$ |
|---|---|---|---|---|---|---|
| | NBS 987 | Ames | LaJolla | NBS 981 | NBS 981 | NBS 981 |
| m | 0.710247 | 0.512123 | 0.511843 | 16.898 | 15.450 | 36.587 |
| $s_a$ | 0.000011 | 0.000010 | 0.000010 | 0.018 | 0.024 | 0.073 |
| n | 23 | 20 | 14 | 23 | 23 | 23 |

Note: m = mean; $s_a$ = analytical standard deviation; $n$ = number of analyses.

isotopic analysis were digested and separated using a modification of the White and Dupré (1986) technique (Harpp, 1994).

Sr isotopic analyses were performed on two thermal ionization mass spectrometers: the new VG Sector 54 TIMS at Cornell and a VG Sector 54 TIMS in the Syracuse University Geology Department. Nd and Pb analyses were conducted solely on the Cornell University mass spectrometer. Standard results are listed in Table 3.

Strontium samples were loaded on single tungsten filaments according to the details in Harpp (1994). Analysis was performed using a dynamic quadruple multicollector program. The mean $^{87}Sr/^{86}Sr$ ratio of 23 analyses of NBS 987 strontium standard was 0.710247. Based on the reproducibility of this standard, the $2\sigma$ analytical uncertainty is estimated at ±0.000021 for individual sample runs. Samples were routinely analyzed a minimum of twice and up to seven times in some cases to verify reproducibility and agreement between instruments. Procedural blanks were negligible.

Neodymium samples were loaded on single rhenium filaments with resin (BioRad AG50W-×12; see Harpp, 1994 for details). Analysis was performed using a dynamic seven collector program. The mean $^{143}Nd/^{144}Nd$ ratio of 14 analyses of the La Jolla isotopic standard was 0.511843. The Ames isotopic standard $^{143}Nd/^{144}Nd$ ratio was 0.512123 for 20 analyses. Both standards yielded a $^{145}Nd/^{144}Nd$ of 0.348426. Based on the standards, the $2\sigma$ analytical uncertainty of the $^{143}Nd/^{144}Nd$ ratios is estimated at ±0.000020 for individual sample runs. Many of the samples were analyzed two or more times to verify reproducibility. Procedural blanks were routinely negligible. Calculation of $\varepsilon_{Nd}$ is based on a $^{143}Nd/^{144}Nd$ ratio of 0.512638 for CHUR (the chondritic uniform reservoir).

Samples for Pb analysis were loaded on single rhenium filaments with silica gel according to Harpp (1994). A static four collector analysis program was used to collect the data. The uncorrected mean $^{206}Pb/^{204}Pb$, $^{207}Pb/^{204}Pb$, and $^{208}Pb/^{204}Pb$ ratios for 23 analyses of NBS 981 were 16.898, 15.450, and 36.587, respectively; the Pb isotope ratios used for correction were 16.937, 15.493, and 36.705, respectively. The $2\sigma$ analytical uncertainties for individual sample analyses are estimated at 0.036 for $^{206}Pb/^{204}Pb$, 0.047 for $^{207}Pb/^{204}Pb$, and 0.146 for

$^{208}Pb/^{204}Pb$. Several samples were analyzed two or more times to verify reproducibility. Procedural blanks for Pb separations were consistently negligible.

## RESULTS

In all geochemical aspects, the Leg 142 samples are typical of N-MORB (see Figs. 2–8 and Tables 4 and 5 for results). Not surprisingly, they resemble samples collected along the 9°–10°N East Pacific Rise segment, including material from the RAIT02 and CHEPR expeditions (Harpp and White, 1990; Harpp et al., 1991; E. Klein, unpubl. data). Lavas erupted at the ridge crest in this area exhibit only a limited range in isotope ratios and trace element concentrations relative to most other EPR segments. The Leg 142 samples, in turn, display considerably less variation than the 9°–10°N EPR axial MORB, or even lavas from a single segment along the superfast-spreading southern EPR (e.g., Prinzhofer et al., 1989, J.J. Mahoney et al., unpubl. data) (see Figs. 2–6).

Although the Leg 142 samples are in general free of visible alteration material, samples were nevertheless leached in HCl prior to isotopic analysis to ensure thorough cleaning. Of the three sets of isotopic ratios measured in this study, $^{87}Sr/^{86}Sr$ is the most sensitive to seawater alteration. The strontium isotope ratio therefore serves as the best indicator of the geological freshness of a material (Verma, 1992).

A number of leaching experiments were performed on selected samples, varying in length of leach time (10–30 min) and strength of the HCl solution (2 vs. 6 M) (see Table 2). Only in the case of powdered samples was there a significant change in $^{87}Sr/^{86}Sr$ after leaching. As a result, powdered samples that were not leached prior to analysis were eliminated from subsequent statistical calculations described below. Neither the leaching time nor the strength of the leachate affected strontium ratios beyond analytical error. In contrast, $^{143}Nd/^{144}Nd$ and Pb isotope ratios were not significantly affected by any level of leaching. These results suggest that the recovered material is fresh and that seawater alteration is not a major factor in the geochemical variations.

In several cases, material was recovered from junk baskets in substantial quantities, consisting of intermixed pieces of glassy and crystalline basalt. Owing to the small sampling interval, the natural assumption is that all fragments originated in the same flow unit. Unfortunately, short of analyzing every morsel of basalt, and considering the poor stratigraphic control, this cannot be proven. To insure that there was no geochemical variation within junk baskets, a random selection of four single glass pieces from Sample 142-864A-1M-6, 0–75
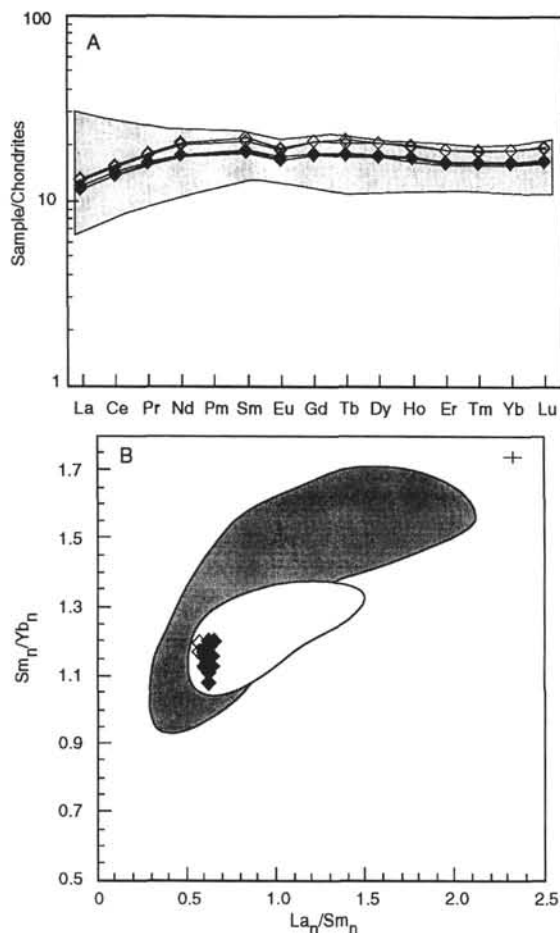
Figure 2. **A.** Chondrite-normalized REE patterns for selected samples. Solid diamonds = Unit 1, open diamonds = Unit 2 (Nakamura et al., 1989). The gray field represents the range in normalized REE concentrations for samples dredged from along the EPR axis between 9° and 10°N on the RAIT02 expedition (Harpp et al., 1991; Batiza and Niu, 1992). **B.** Ratios of chondrite-normalized REE abundances; symbols as in **A**. The open field encompasses all data from 9°–10°N on the EPR axis (see **A**); the gray field includes data from the EPR segment at 12°50′N (Prinzhofer et al., 1989). Error bars represent one standard deviation analytical precision.



Figure 3. **A.** Y/Zr vs. Zr/Nb. **B.** $Nd_n/Sm_n$ vs. Y/Zr. Solid diamonds = Unit 1; open diamonds = Unit 2; open field = 9°–10°N axial EPR dredge samples (Harpp et al., 1991; Batiza and Niu, 1992); gray field = 12°50′N EPR segment data (Prinzhofer et al., 1989); striped field = data from the 20.88°–21.43°S segment of the EPR (J.J. Mahoney et al., unpubl. data). Error bars represent one standard deviation analytical precision.
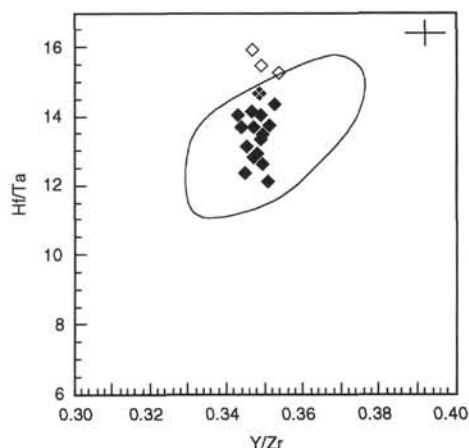


Figure 4. Y/Zr vs. Hf/Ta. Symbols as in Figure 3. Error bars represent one standard deviation analytical precision.

cm was examined for Sr and Nd isotopic ratios (Table 2). Variation between samples was negligible for both isotope ratios.

Some individual basalt fragments from the junk baskets consist of both glassy and coarser-grained crystalline portions. One such sample, 2 cm in length from glassy to crystalline ends (142-864A-1M-6, 75–135 cm) was separated into its glass and crystalline components and each was measured for $^{87}Sr/^{86}Sr$. The difference between the samples was insignificant, at 0.000012, as would be expected (Table 2). In addition, this exercise established that there is no bias in the isotopic analyses from crystalline vs. glassy basalt matrices.

Several samples exhibit anomalous trace element concentrations: 142-864A-1M-2 ("contam") has high Ba and low REEs; 864A-1M-2, 0–35 cm and 864A-4Z-1, 9–15 cm also have high Ba; 864A-4Z-1 (Piece #2) has high Ta values. The errors are probably not analytical because the results were confirmed in replicate analyses. It is unlikely that the samples were contaminated in the Cornell laboratory, because there are no major sources of Ba, REEs, or Ta available. It is possible, however, that these samples were contaminated during han-
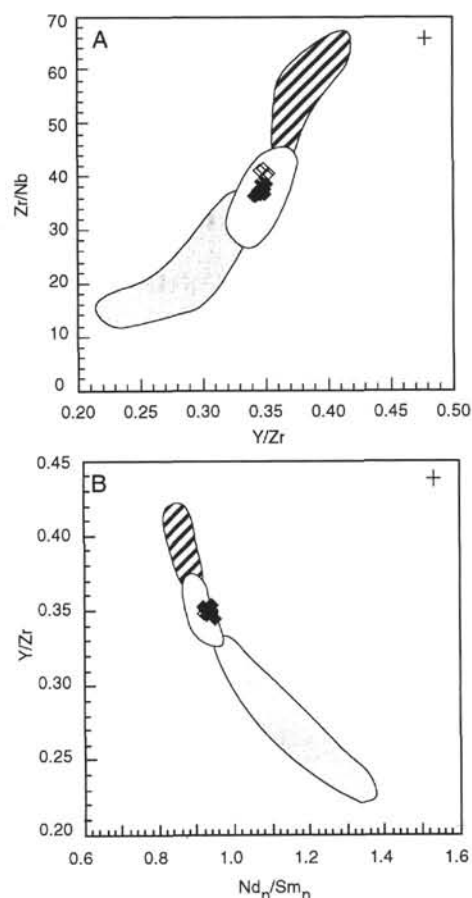
dling aboard *JOIDES Resolution*. The REE concentrations of 142-864A-1M-2 ("contam") may have been diluted with low-REE content material during shipboard grinding experiments (Shipboard Scientific Party, 1993a). Plausible sources for both Ba and Ta con-

Figure 5. Radiogenic isotope ratios. **A.** $^{87}Sr/^{86}Sr$ vs. $\varepsilon_{Nd}$ for the EPR. Diamonds = all Leg 142 samples; fields as in Figure 2. **B.** Close-up view of samples from near 9°30′N on the EPR. Diamonds = Leg 142 data; crosses = RAIT02 dredge samples (Harpp et al., 1991); open triangles = data from the CHEPR cruise (E. Klein, unpubl. data). Error bars represent one standard deviation analytical precision.
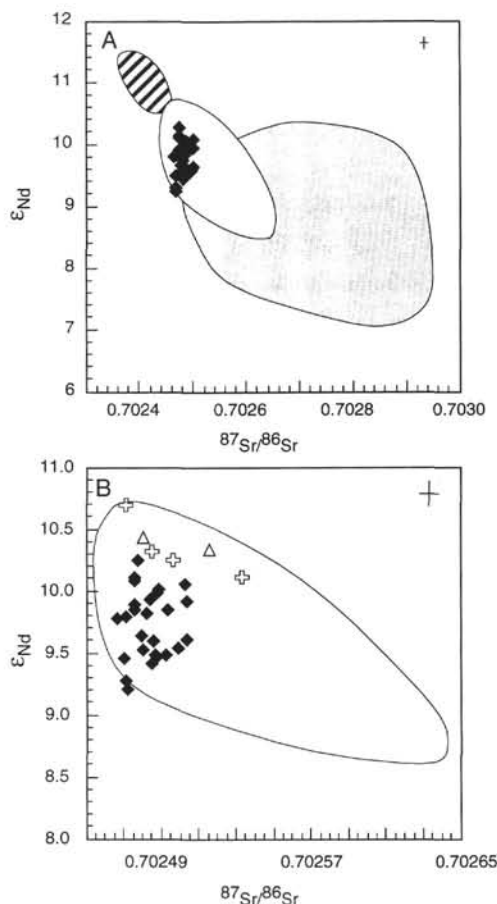


Figure 6. Lead isotope data; fields as in Figure 2. Diamonds = all Leg 142 data. Error bars represent one standard deviation analytical precision.

tamination were used in the drilling process. Barite was used to fill voids in the ballast of the hard-rock guidebase; all recovered samples passed through the guidebase. The Ba contamination may result from small amounts of barite that were not completely removed by shipboard cleaning procedures. The drill bits utilized to initiate drilling included substantial amounts of tungsten carbide; unpurified W commonly contains some Ta (e.g., Hurlbut and Klein, 1977). Under the arduous drilling conditions, many drill bits were severely damaged. Some of the fragments from the drill bits may have escaped the shipboard cleaning process and thus may have mixed with the sample during grinding, resulting in an elevated Ta level in the 142-864A-4Z-1 (Piece #2) powder. Suspected contamination values were removed from the data sets prior to statistical analysis.

## STATISTICAL ANALYSIS

The goals of this study are twofold: (1) to quantify the magnitude of geochemical variation within a single eruptive unit at a mid-ocean ridge and (2) to verify through trace element and isotopic analysis the conclusion reached by the Shipboard Scientific Party that two chemically distinct units were sampled on Leg 142. Results listed in Tables 4 and 5 clearly show that the geochemical variation between samples is small and, in many cases, comparable to analytical uncertainty. Thus, 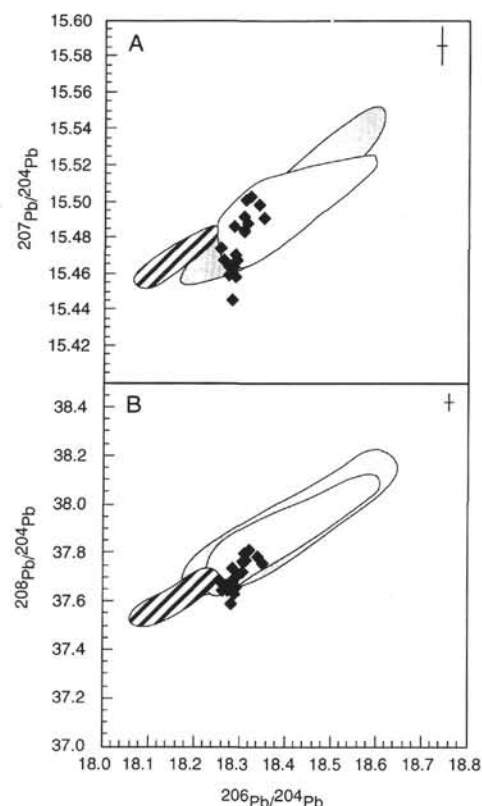the first task is to determine how much of the observed chemical and isotopic variation is real and how much is attributable to analytical factors, which requires the application of statistical tests.

## Significance of Geochemical Variation

One of the basic assumptions in many statistical methods is that the data are drawn from a population with a normal distribution (Miller and Miller, 1992; Snedecor and Cochran, 1989; Allègre et al., 1984). Although it is not possible to prove that the distribution of either isotope ratio or elemental concentration data within an eruptive unit is normal, the central limit theorem states that even if the original population is not normal, the sampling distribution of the mean approaches a normal distribution as sampling frequency increases (e.g., Snedecor and Cochran, 1989). Therefore it is reasonable to accept the distribution of geochemical variations within individual geological units as approximately normal, permitting the application of statistical significance tests.

The total variation within a data set is best described quantitatively with the total variance, $s_t^2$. The variance is the most sensitive measure of homogeneity and consists of the sum or nearly the sum of two primary components: (1) the variance resulting from natural causes in the geological system ($s_n^2$); that is, the variation of interest in this study; and (2) the variance superimposed on natural variations by analytical procedures ($s_a^2$) (Shaw and Cruft, 1967):

$$s_t^2 = s_n^2 + s_a^2 .$$

Because the geochemical variations between samples are small, the first step is to assess total variation in the data set relative to that caused by random analytical factors. If total variation is significantly larger than that caused by analytical procedures, then a significant
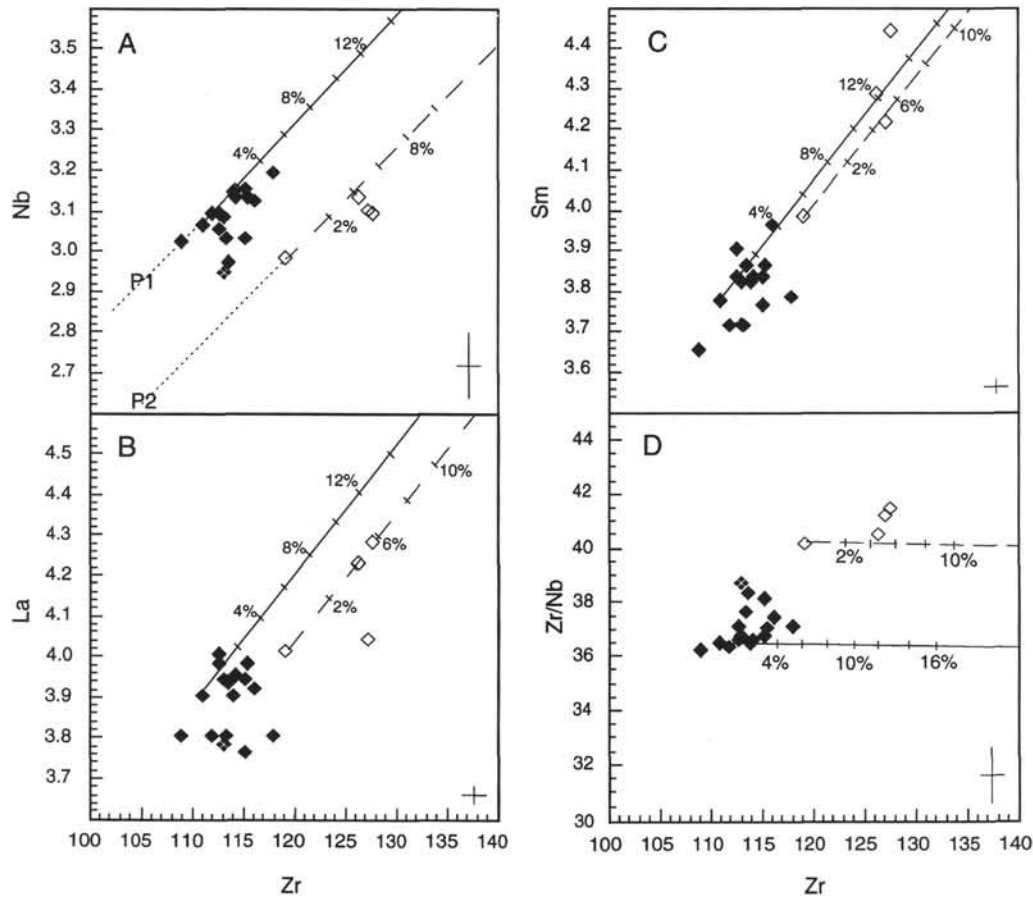
Figure 7. Variation diagrams of selected elements concentrations vs. Zr contents. Values are in ppm. Solid lines represent calculated fractionation pathways for simple low-pressure fractional crystallization for a closed magma chamber, with Sample 142-864A-1M-3, 0–35 cm (powdered), as parent melt. Dashed lines were calculated with Sample 142-864A-4Z-1 (Piece #2) (powdered) as the parent lava. Tick marks represent 2% fractional crystallization increments. Symbols as in Figure 3. In **A.**, P1 and P2 represent the parental melts of Units 1 and 2, respectively, to illustrate relative compositions. P1 and P2 are located along extrapolations of the fractionation pathways for the two units, and are only for illustrative purposes. Error bars represent one standard deviation analytical precision.

portion of the variation is real and can be examined in detail for patterns in the data.

A two-tailed F test was employed for the comparison of $s_t^2$ to $s_a^2$, with the null hypothesis that $s_t^2$ and $s_a^2$ are equal and all samples are identical. Total variance in the data $s_t^2$ is calculated for each geochemical measurement (Snedecor and Cochran, 1989; Miller and Miller, 1992). The analytical variance ($s_a^2$) is adequately estimated from the standard analyses for ICP-MS for the REEs, Ba, Y, Zr, Nb, Hf, and Ta; TIMS for isotopic ratios; and shipboard XRF for the major elements Cr, Ni, V, Cu, Zn, and Sr. The results of the F tests at the 5% probability level, with calculated ($F_c$) and tabulated values ($F_{5\%}$) for the trace and major element concentrations and isotope ratios, are listed in Tables 4 and 5.

The F tests show that the null hypothesis cannot be rejected at a 5% probability level for all isotope ratios ($^{87}Sr/^{86}Sr$, $^{143}Nd/^{144}Nd$, $^{206}Pb/^{204}Pb$, $^{207}Pb/^{204}Pb$, $^{208}Pb/^{204}Pb$), as well as for Nb, Ta, Sr and most of the major elements (see Tables 4, 5, and 6). In these cases, geological variations cannot be distinguished from analytical error and samples should be considered uniform insofar as can be detected with present instrumental techniques. No further statistical tests will be performed on these geochemical parameters.

In contrast, the F tests reveal that the null hypothesis can be rejected at the 5% level for the remaining trace elements, Ba, the REEs, Y, Zr, Hf, Cr, Ni, V, Cu, and Zn as well as major oxides $TiO_2$, $Fe_2O_3$, CaO, and $K_2O$ (see Tables 4, 5, and 6). The bulk of the measured trace elements exhibit variation significantly greater than analytical uncertainty and thus merit further investigation.

## Distribution of Geochemical Variation

The next step is to determine how the natural fluctuations of the elements are distributed between the samples. The primary questions of interest are: (1) does the data fall into natural groups that are consistent for all the geochemical measurements; and (2) if so, is the original shipboard assignment of two lithologic units appropriate?

Clustering techniques are mathematical classification methods designed to sort data into groups such that the samples within a cluster are more similar to each other than they are to samples in other clusters. While there are many variations of cluster analysis, there is no general agreement on the best method, and it is used primarily as an exploratory tool. A series of hierarchical cluster analyses was performed on the Leg 142 data set, including all the major and trace element concentrations. The method of complete-linkage distance clustering was employed (Davis, 1986). In all cases, the samples cluster into two groups, corresponding largely to the two-unit Shipboard classification scheme. A single Unit 2 sample, 142-864A-5Z-1, 12–15 cm, repeatedly clusters with Unit 1 material. With this exception, the division of the samples into two and only two lithologic units appears to be justified; no other natural divisions seem to exist in the data set when the interactions among all the element compositions are considered.

In terms of the concentrations determined in this laboratory, Unit 1 samples have lower average contents of the REEs, Hf, Y, and Zr than Unit 2. Barium exhibits the opposite behavior, with lower mean concentrations in Unit 2 than in Unit 1. As described in the *Initial Re-*
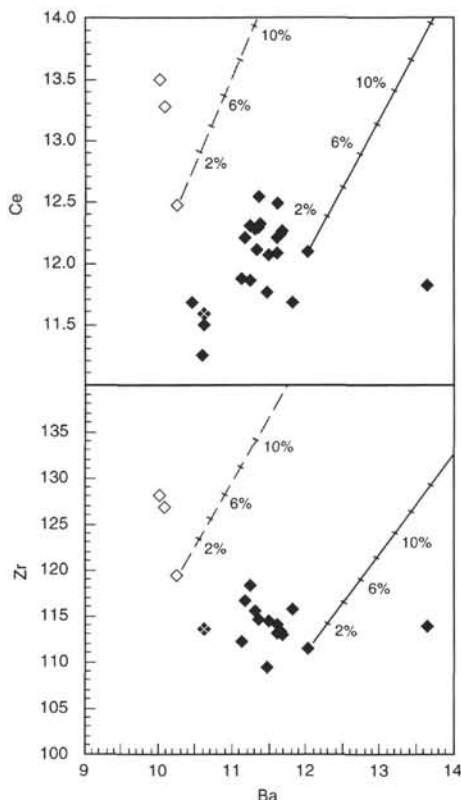
15

Figure 8. Variation diagrams of Ce and Zr concentrations vs. Ba contents. Values are in ppm. Solid diamonds = Unit 1; open diamonds = Unit 2.

*ports* (Shipboard Scientific Party, 1993b), Unit 1 is also characterized by higher mean CaO, Cr, Ni, and Cu, and by lower mean $TiO_2$, $Fe_2O_3$, V, and Zn. Units 1 and 2 have equal $K_2O$ contents. With the exception of some of the elements determined by XRF, Unit 2 samples cover a larger range in concentrations than Unit 1.

Despite being assigned to Unit 2 because it was recovered at one of the greatest drilling depths (>12 m), Sample 864A-5Z-1, 12–15 cm appears more similar to Unit 1 geochemically. In reality, it could have originated anywhere from 0 to 12 m below the seafloor, a result of the fragmented nature of the basalt at the drilling site; rubble could simply have fallen into the hole from above before being lodged in the drill bit. When viewed on element-element plots (Fig. 7), Sample 864A-5Z-1, 12–15 cm usually falls in the midst of the Unit 1 field. In the absence of better stratigraphic control, major element concentrations, and thin section descriptions for this particular fragment, Sample 864A-5Z-1, 12–15 cm will be grouped with Unit 1 material for subsequent statistical procedures.

Having established the existence of two primary geochemical groups, a more quantitative statistical test is needed to examine causes of variation in the data set. A one-way factorial analysis of variance (ANOVA) was performed on each element with significant variation (REEs, Ba, Y, Zr, and Hf from ICP-MS, as well as Cr, Ni, V, Cu, Zn, $TiO_2$, $Fe_2O_3$, CaO, and $K_2O$ from shipboard XRF) to determine if the variation could be attributed to a geochemical distinction between Unit 1 and Unit 2 (Miller and Miller, 1992). Results are listed in Table 7. The probability values in Table 7 represent the likelihood that the observed difference between the means for Unit 1 and Unit 2 could occur by chance if the means were actually equal. For most elements, Unit 1 appears to be distinguishable at better than a ~4% probability from Unit 2. Units 1 and 2 are not statistically distinguishable on the basis of $K_2O$, Ni, Cu, or Zn.

A second factor that was tested as a possible control of variation is the geological form of the sample (crystalline vs. glassy). This procedure was used exclusively on the elements determined by ICP-MS; only powders were measured by XRF. No significant effect was found, indicating that glassy and crystalline materials exhibit the same geochemical variations within units. This suggests that there is no advantage to analyzing glassy over fresh crystalline interiors.

In summary, the Leg 142 samples are indistinguishable in terms of their Sr, Nd, and Pb isotopes, Nb, Ta, Sr, Ni, Cu, and Zn concentrations and most of the major oxides. In contrast, the remaining concentration data including the rare earth elements, Ba, Y, Zr, Hf, Cr, V, CaO, and $TiO_2$, can be divided into two statistically-separate groups, corresponding largely to the original assignments of Unit 1 and Unit 2 (see Tables 4 and 5).

## DISCUSSION

### Comparison with 9°–10°N Axial Samples

Several along-axis geochemical studies have been conducted on the East Pacific Rise, including some with high sampling densities (e.g., MacDougall and Lugmair, 1986; Hamelin et al., 1984; Sinton et al., 1991; Mahoney et al., unpubl. data; Prinzhofer et al., 1989; Hekinian et al., 1989). Of particular interest is the ridge segment that includes the drill site, 9°17'–9°51'N. Detailed geophysical studies in the area suggest that this segment is underlain by a single, axially continuous magma chamber (e.g., Detrick et al., 1987; Toomey et al., 1990; Kent et al., 1990). Dredging undertaken during the RAIT02 Cruise (Batiza and Niu, 1992; Harpp and White, 1990) was designed to examine geochemical variations along the strike of the axial magma chamber (AMC). Dredges were located approximately 1.8 km apart at the axis (Batiza and Niu, 1992). These closely spaced samples have been analyzed for Sr, Nd, and Pb isotopes as well as a variety of trace element concentrations (Harpp, 1994). In Figures 2 through 6, the Leg 142 samples are plotted alongside axial lavas from 9°–10°N.

Batiza and Niu (1992) explained the major and trace element variations between 9° and 10°N with a chemically-zoned magma chamber model, in which all material originates from the same source. Magma cools and crystallizes to different extents as it migrates along the ridge away from the single injection point located at the axial high near 9°48'N. The isotopic data, however, exhibit subtle but significant variation in Sr, Nd, and Pb ratios in the form of a smooth, undulating curve along the axis. As a result, lavas erupted along the segment cannot be related simply by fractional crystallization as stated by Batiza and Niu (1992). More in concert with the observed variations, the magma chamber may be periodically replenished with isotopically-distinct magma batches, either at different times from a single injection point or, more likely, at different locations along the ridge. The material would then be subjected to limited along-strike mixing in the AMC, resulting in a smooth variation in isotopic signals along the axis. The question at this point becomes what scale of isotopic variation along a ridge is significant? Are the variations observed on the scale of tens of kilometers no greater than the ones observed on the scale of meters? Are the variations between geographically distant eruptive units no greater than the variations within a single flow? If the answer to either of the latter questions is yes, then the observed regional variations can be regarded as geologically meaningless and one could reasonably conclude that magmas erupted within this ridge segment are geologically homogeneous.

The data from the Leg 142 study is of immediate relevance to this issue. The range of geochemical variations at a single location on the ridge, as determined in this study, can be compared to the spread in the data from samples collected along the axis. In fact, the axial samples exhibit a significantly larger variation in all aspects of their geochemistry than the subsurface ODP lavas (Figs. 2 through 6).

Therefore, the subtle variations along the ridge axis are significant and can be attributed to real geological phenomena such as differences in melt supply composition, possibly accompanied by limited along-axis mixing in the magma chamber.

## Geochemical Differences Between Unit 1 and Unit 2

Material from Leg 142 is isotopically homogeneous but can be divided into two distinct groups based on the concentrations of several elements. Niobium, Ta, Sr, and most of the major oxides, however, do not exhibit detectable variations beyond analytical error. In addition, $K_2O$, Cu, Ni, and Zn display significant variations but cannot be used to distinguish between the units. These observations bring several questions to mind: (1) why is there a lack of correlation between isotope and trace element variations; (2) what process is responsible for the geochemical differences between Units 1 and 2; and, finally, (3) why do only selected elements show differences between the units?

It is a basic assumption in geochemistry that variations in isotopic ratios of basalt reflect variations in the isotopic composition of the source, as well as any mixing en route to the surface of melts derived from isotopically-distinct sources. In contrast, elemental concentrations are affected not only by source and mixing factors but also by melting and recrystallization processes. Melting and crystallization processes must be responsible for the distinction between Unit 1 and Unit 2. There are three primary scenarios to consider: (1) Unit 1 and Unit 2 originate from distinct sources that differ in their elemental compositions but are isotopically identical; (2) Units 1 and 2 share a common source and the same parental melt but have evolved remotely along different shallow fractionation pathways; and, (3) Units 1 and 2 are the result of distinct parental melts that have evolved from the same source via different melt generation processes.

The first option is conceivable but unrealistic. Long-standing differences in trace element compositions lead inevitably to variations in mantle isotopic ratios, making the existence of two sources with similar isotope ratios but different trace element characteristics unlikely.

Alternatively, based on their similar compositions and in particular on their identical isotopic ratios, Units 1 and 2 may have been produced contemporaneously and share a common parental melt. How then do the subtle variations in trace element concentrations arise? The melts must have evolved differently since their production. Shallow-level processes in the magma chamber including low-pressure fractionation and crystal accumulation can affect trace element abundances in melts, and warrant further investigation.

As the Leg 142 Shipboard Scientific Party points out in the *Initial Reports* volume (1993b), all the recovered material falls along the general fractionation trend established by other EPR glasses collected near 9°30'N (Batiza and Niu, 1992; Harpp et al., 1991). Batiza and Niu (1992) conclude that most of these lavas are related through low-pressure fractional crystallization and were produced by approximately 18% partial melting of a depleted mantle source. While the dredged samples provide a reasonable first approximation for a fractionation pathway, they do not accurately reproduce the distribution of the Leg 142 compositions.

If all the Leg 142 material is related simply by low-pressure fractional crystallization from a common parent, it should be possible to reproduce both Unit 1 and Unit 2 compositions by calculating a fractionation pathway from the most primitive sample of the group. The sample that must be used as the parent lava in the calculations is certainly not as primitive as the true original melt, but it should nevertheless result in the same fractionation curve; the starting point will simply be located at a more evolved composition along the same differentiation path.

The Mixnfrac program developed by R.L. Nielsen (1988) was employed to model low-pressure fractional crystallization of the Leg 142 basalts in a closed magma chamber. This program simulates the effect of fractionation on major and trace elements with a model based on compositionally-independent trace element partition coefficients in tandem with a major element phase equilibria model (Nielsen and Dungan, 1983; Nielsen, 1985; Nielsen, 1988). All major and trace element data were considered in the calculations. Typical crystallizing mineral assemblages for the Leg 142 samples consist of olivine and plagioclase.

The most primitive Unit 1 sample for which all the major and trace element concentrations were available, 142-864A-1M-3, 0–35 cm (powdered), was used as the initial melt to generate a fractionation pathway. The calculated low-pressure fractional crystallization line does pass through some of the Unit 1 data, but it does not reproduce Unit 2 compositions. The calculation was repeated using Unit 2 Sample 142-864A-4Z-1 (Piece #2, powdered). Similarly, some Unit 2 samples lie along the fractionation curve but Unit 1 samples do not (Fig. 7). The above calculations were performed assuming a closed magma chamber. Nielsen's program (1988) also permits the simulation of varying proportions of recharge and eruption. Regardless of the amounts of recharge and/or eruption, a Unit 1 composition could not be made to reproduce Unit 2 lavas, and vice versa. As illustrated in Figures 2, 3, 4, 7 and 8, Units 1 and 2 exhibit distinct, unrelated geochemical characteristics, cannot be related to each other through simple low-pressure fractional crystallization, and must have evolved instead from geochemically distinct parental melts.

Another shallow-level process, crystal accumulation, cannot explain the relationship between the units either. Unit 2 is more phenocryst rich than Unit 1, yet has generally higher incompatible element concentrations. In addition, the two groups of samples lie on distinct fractionation pathways. There is therefore no combination of appropriate minerals that will successfully reproduce both the major and trace element abundances of Unit 2 from Unit 1 by simple crystal accumulation.

Can intra-unit geochemical relationships be explained by straightforward low-pressure fractional crystallization? In Figures 7 and 8 the degrees of fractional crystallization are indicated along the fractionation trends. Most Unit 2 samples fall close to the fractionation trends on some element-element plots, although the fit ranges from imperfect to nonexistent; Unit 1 samples fail to follow any obvious trend, clustering instead in a shotgun pattern at the origin of the fractionation lines.

Shallow-level phenomena do not appear to be the cause of the geochemical variations. Because the AMC is located between 1 and 3 km beneath the ridge (Detrick et al., 1987; Sinton and Detrick, 1992), processes in the axial magma chamber must not be the source for the differentiation between Units 1 and 2. More likely, Unit 1 and Unit 2 melts were injected into the AMC as geochemically distinct batches.

Results from a detailed textural study of plagioclase phenocrysts from Leg 142 indicate that prior to entering the melt lens, the crystals encountered a range of liquid compositions comparable to that observed throughout the 9°–10°N segment (Brophy and Allan, this volume). The authors propose that as the liquids migrated upward, they passed through a network of discrete melt bodies in the mush zone underlying the AMC (Sinton and Detrick, 1992), undergoing a series of in situ mixing and fractionation events (Brophy, this volume). Zonation in the plagioclase crystals also suggests the liquids were exposed to vigorous convection once injected into the melt lens.

According to the conclusions of Brophy and Allan (this volume), it will not be possible to discern precise fractionation trends from the glass and whole rock analyses presented in this paper. Instead, the samples represent the average compositions of the liquids in the melt lens at the time of eruption. The geochemical variations within each sample originate from complex fractionation processes, but will be partially obscured by subsequent mixing in the magma lens.

There are no geochemical relationships within Unit 1 lavas that suggest shallow-level mixing processes. Instead, Unit 1 data forms a tight cluster on most variation diagrams and can be considered homo-

Table 4. Selected trace element concentrations determined by ICP-MS, Site 864.

| Core, section, interval (cm) | Sample type | Unit | Ba | La | Ce | Pr | Nd | Sm | Eu | Gd | Tb | Dy | Ho | Er |
|---|---|---|---|---|---|---|---|---|---|---|---|---|---|---|---|
| 142-864A- | | | | | | | | | | | | | | |
| 1M-1, 1–10 | Powder | 1 | 10.5 | 3.82 | 11.67 | 2.04 | 10.83 | 3.58 | 1.26 | 4.69 | 0.94 | 5.74 | 1.27 | 3.44 |
| 1M-2, "contam" | Powder | 1 | 16.2 | 3.31 | 10.36 | 1.78 | 9.45 | 3.16 | 1.14 | 4.25 | 0.84 | 5.19 | 1.13 | 3.13 |
| 1M-2, 0–35 (a) | Powder | 1 | 10.6 | 3.89 | 11.50 | 1.98 | 10.32 | 3.55 | 1.28 | 4.67 | 0.92 | 5.58 | 1.22 | 3.36 |
| 1M-2, 0–35 (b) | Powder | 1 | 11.7 | 3.94 | 12.23 | 2.09 | 11.21 | 3.82 | 1.32 | 4.94 | 0.99 | 6.02 | 1.32 | 3.58 |
| 1M-2, 0–35 | Glass | 1 | 31.5 | 3.98 | 12.36 | 2.13 | 11.23 | 3.86 | 1.31 | 5.17 | 1.00 | 6.19 | 1.36 | 3.75 |
| 1M-2, 54–84 | Crystalline | 1 | 11.8 | 3.76 | 11.67 | 2.02 | 10.84 | 3.76 | 1.26 | 4.96 | 0.93 | 5.90 | 1.32 | 3.57 |
| 1M-2, 100–150 | Crystalline | 1 | 11.3 | 3.94 | 12.27 | 2.11 | 11.16 | 3.83 | 1.30 | 5.07 | 1.00 | 6.19 | 1.37 | 3.78 |
| 1M-3, 0–35 | Glass | 1 | 12.1 | 3.90 | 12.09 | 2.09 | 11.10 | 3.77 | 1.30 | 5.03 | 0.99 | 6.05 | 1.34 | 3.69 |
| 1M-3 ,0–35 | Powder | 1 | 10.6 | 3.70 | 11.25 | 1.90 | 10.17 | 3.51 | 1.21 | 4.78 | 0.95 | 5.88 | 1.32 | 3.74 |
| 1M-3, 54–84 | Crystalline | 1 | 11.2 | 3.80 | 11.87 | 2.05 | 11.05 | 3.71 | 1.28 | 4.92 | 0.97 | 5.98 | 1.33 | 3.61 |
| 1M-3, 54–84 | Powder | 1 | 11.4 | 4.00 | 12.10 | 2.03 | 10.89 | 3.72 | 1.28 | 4.91 | 0.98 | 6.11 | 1.33 | 3.81 |
| 1M-3, 100–150 | Crystalline | 1 | 11.2 | 3.92 | 12.20 | 2.10 | 11.38 | 3.96 | 1.31 | 5.05 | 1.00 | 5.97 | 1.34 | 3.61 |
| 1M-3, 100–150 | Powder | 1 | 11.4 | 3.97 | 12.53 | 2.12 | 11.06 | 3.81 | 1.35 | 5.03 | 0.98 | 6.12 | 1.33 | 3.61 |
| 1M-4, 0–9 | Powder | 1 | 11.3 | 3.99 | 12.30 | 2.14 | 11.44 | 3.87 | 1.35 | 5.15 | 1.03 | 6.30 | 1.36 | 3.73 |
| 1M-5, 0–100 | Crystalline** | 1 | 11.5 | 3.90 | 12.06 | 2.07 | 11.07 | 3.82 | 1.29 | 4.99 | 0.98 | 5.93 | 1.31 | 3.56 |
| 1M-5, 0–100 | Glass* | 1 | 11.3 | 3.80 | 11.85 | 2.04 | 10.92 | 3.78 | 1.27 | 4.91 | 0.97 | 5.87 | 1.29 | 3.57 |
| 1M-5, 0–100 | Powder | 1 | 11.7 | 4.00 | 12.26 | 2.09 | 11.19 | 3.83 | 1.30 | 5.07 | 1.01 | 6.14 | 1.34 | 3.69 |
| 1M-6, 0–75 | Powder | 1 | 11.4 | 4.06 | 12.32 | 2.14 | 11.31 | 3.92 | 1.34 | 5.23 | 1.03 | 6.31 | 1.34 | 3.77 |
| 1M-6, 0–75 | Glass | 1 | 11.6 | 3.98 | 12.48 | 2.15 | 11.51 | 3.90 | 1.34 | 5.14 | 1.01 | 6.10 | 1.34 | 3.69 |
| 1M-6, 75–135 | Crystalline* | 1 | 11.5 | 3.80 | 11.76 | 2.03 | 10.82 | 3.65 | 1.26 | 4.85 | 0.95 | 5.90 | 1.26 | 3.50 |
| 1M-6, 75–135 | Crystalline** | 1 | 11.4 | 3.95 | 12.28 | 2.13 | 11.29 | 3.83 | 1.31 | 5.13 | 1.00 | 6.16 | 1.32 | 3.68 |
| 1M-6, 75–135 | Powder | 1 | 11.6 | 3.94 | 12.08 | 2.12 | 10.99 | 3.77 | 1.29 | 5.15 | 1.02 | 6.16 | 1.34 | 3.71 |
| 142-864B- | | | | | | | | | | | | | | |
| 2W-1, 0–4 | Crystalline | 1 | 13.7 | 3.80 | 11.82 | 2.06 | 10.93 | 3.71 | 1.27 | 4.95 | 0.96 | 5.94 | 1.33 | 3.59 |
| 2W-1, 16–18 | Powder | 1 | 11.6 | 3.93 | 12.21 | 2.11 | 11.35 | 3.86 | 1.32 | 5.11 | 1.01 | 6.26 | 1.41 | 3.80 |
| 142-864A- | | | | | | | | | | | | | | |
| 4Z-1, (Piece #2) | Powder | 2 | 10.3 | 4.01 | 12.47 | 2.15 | 11.68 | 3.98 | 1.35 | 5.40 | 1.06 | 6.49 | 1.44 | 3.98 |
| 4Z-1, 9–15 | Crystalline | 2 | 22.4 | 4.04 | 12.87 | 2.23 | 12.06 | 4.21 | 1.40 | 5.49 | 1.10 | 6.68 | 1.48 | 3.98 |
| 5Z-1, 5–9 | Crystalline | 2 | 10.0 | 4.28 | 13.49 | 2.37 | 12.97 | 4.44 | 1.48 | 5.77 | 1.16 | 7.04 | 1.51 | 4.24 |
| 5Z-1, 12–15 | Crystalline | 2(1) | 10.6 | 3.78 | 11.58 | 2.05 | 10.89 | 3.71 | 1.32 | 4.98 | 0.95 | 5.95 | 1.30 | 3.61 |
| 5Z-1, 24–30 | Powder | 2 | 10.1 | 4.23 | 13.27 | 2.29 | 12.57 | 4.28 | 1.45 | 5.79 | 1.12 | 6.98 | 1.56 | 4.26 |
| $s_t$ | | | 0.73 | 0.13 | 0.49 | 0.09 | 0.57 | 0.20 | 0.06 | 0.27 | 0.06 | 0.33 | 0.07 | 0.21 |
| $n$ | | | 26 | 28 | 28 | 28 | 28 | 28 | 28 | 28 | 28 | 28 | 28 | 28 |
| $F_c$ | | | 6.00 | 5.12 | 39.06 | 14.04 | 43.41 | 19.04 | 8.53 | 7.84 | 13.65 | 10.78 | 5.25 | 9.61 |
| $F_{5\%}$ | | | 1.97 | 1.95 | 1.95 | 1.95 | 1.95 | 1.95 | 1.95 | 1.95 | 1.95 | 1.95 | 1.95 | 1.95 |
| $s_n$ | | | 0.67 | 0.12 | 0.48 | 0.09 | 0.57 | 0.20 | 0.05 | 0.25 | 0.05 | 0.31 | 0.07 | 0.19 |
| | | | BIR | BIR | BIR | BIR | BIR | BIR | BIR | BIR | BIR | BIR | BIR | BIR |
| Unit 1 | | | | | | | | | | | | | | |
| $m_1$ | | | 11.4 | 3.90 | 12.03 | 2.07 | 11.04 | 3.77 | 1.30 | 5.00 | 0.98 | 6.03 | 1.32 | 3.64 |
| $s_1$ | | | 0.63 | 0.09 | 0.33 | 0.06 | 0.32 | 0.11 | 0.03 | 0.15 | 0.03 | 0.18 | 0.04 | 0.11 |
| $n$ | | | 23 | 24 | 24 | 24 | 24 | 24 | 24 | 24 | 24 | 24 | 24 | 24 |
| Unit 2 | | | | | | | | | | | | | | |
| $m_2$ | | | 10.2 | 4.14 | 13.03 | 2.26 | 12.32 | 4.23 | 1.42 | 5.61 | 1.11 | 6.80 | 1.50 | 4.12 |
| $s_2$ | | | 0.12 | 0.13 | 0.45 | 0.09 | 0.57 | 0.19 | 0.06 | 0.20 | 0.04 | 0.26 | 0.05 | 0.16 |
| $n$ | | | 3 | 4 | 4 | 4 | 4 | 4 | 4 | 4 | 4 | 4 | 4 | 4 |
| $s_m$ max | | | 0.21 | 0.04 | 0.06 | 0.02 | 0.06 | 0.03 | 0.01 | 0.07 | 0.01 | 0.07 | 0.02 | 0.05 |

Note: Values in ppm. * = small fragment; ** = large fragment; 2(1) = sample originally assigned to Unit 2 but reassigned to Unit 1 based on statistical tests (included with Unit 1 for mean and standard deviation calculations); $s_t$ = total standard deviation in the data set; $n$ = count; $F_c$ = calculated F statistic; $F_{5\%}$ = tabulated F statistic for a two-tailed test at 5% probability, with degrees of freedom consisting of the number of observations in the data set less one in the numerator, and the number of observations of the standard less one in the denominator, for each geochemical measurement; $s_n$ = estimate of the standard deviation attributable to natural or geological factors calculated as: $s_n = \left[s_t^2 - s_a^2\right]^{1/2}$; BIR, BHVO, and W2 are the ICP-MS standards used in statistical calculations for each element; $m_1$ and $m_2$ = means for Unit 1 and Unit 2, respectively; $s_1$ and $s_2$ = standard deviations of Units 1 and 2, respectively; $s_m$(max) = maximum analytical standard error of the mean for each sample ($s_a/\sqrt{x}$, where x is the number of replicate analyses); Sample 142-864A-1M-2, "contam" (powdered) is not included in any of the calculations; the suspected contamination values of Ba and Ta (see text) also are not included in any calculations.

geneous. Material from Unit 2, however, has a greater concentration range and most samples fall along a trend reminiscent of a mixing line (see Figs. 7 and 8). Four samples in particular exhibit potential mixing relationships: Samples 142-864A-4Z-1, (Piece #2), 864A-5Z-1, 5–9 cm, 864A-5Z-1, 24–30 cm, and 864A-5Z-1, 12–15 cm, the fragment originally grouped with Unit 2 but reassigned to Unit 1 based on elemental concentrations. These lavas spread along a trend between two end members with compositions typical of Unit 1 material and Sample 142-864A-5Z-1, 5–9 cm. Unfortunately, positions of the samples relative to each other vary depending on the elements being examined, which is inconsistent with simple binary mixing (Langmuir et al., 1978). The geochemical relationships within Unit 2 indicate instead a complex mixing process involving a variety of liquids with similar compositions.

## Model for Evolution of Unit 1 and Unit 2

The evidence suggests the following scenario. Unit 1 and 2 samples are derived from two, or, more likely, a spectrum of distinct pa-

rental melts. The parental melts share the same mantle source, as evidenced by their equivalent isotopic compositions. The parental melts evolve via different melt generation paths. Several magma production processes could result in subtle variations in elemental compositions, including high-pressure fractional crystallization, differences in pressure and temperature of melt generation, which in turn affect distribution coefficients (Nielsen et al., 1992), the pathway taken by the evolving melt through the mantle melting regime (Klein and Langmuir, 1987), and even simple differences in the extent of melting. Incompatible element concentrations will be affected to a greater extent by variations in melting processes than the major and more compatible trace elements, a phenomenon reflected in the results of this study. Units 1 and 2 differ significantly in their incompatible element contents, including the REEs, Ba, Hf, Y, and Zr. In terms of most of the major and more compatible elements such as Ni and Cu, in contrast, the two units are indistinguishable.

As the melts migrate upward through the mush zone, they undergo a series of in situ fractionation processes, interacting with a network of discrete liquid bodies. The melts enter the magma chamber

Table 4 (continued).

| Tm | Yb | Lu | Y | Zr | Nb | Hf | Ta |
|---|---|---|---|---|---|---|---|
| 0.55 | 3.36 | 0.52 | | | | | |
| 0.48 | 3.09 | 0.49 | | | | | |
| 0.54 | 3.22 | 0.51 | | | | | |
| 0.56 | 3.54 | 0.56 | 39.5 | 113 | 3.08 | 2.81 | 0.22 |
| 0.59 | 3.65 | 0.60 | 40.2 | 116 | 3.13 | 2.97 | 0.23 |
| 0.57 | 3.53 | 0.54 | 40.4 | 116 | 3.03 | 2.67 | 0.20 |
| 0.59 | 3.67 | 0.60 | 40.2 | 116 | 3.15 | 3.01 | 0.21 |
| 0.59 | 3.59 | 0.58 | 38.9 | 111 | 3.06 | 2.76 | 0.20 |
| 0.57 | 3.54 | 0.58 | | | | | |
| 0.57 | 3.58 | 0.56 | 38.6 | 112 | 3.09 | 2.79 | 0.20 |
| 0.58 | 3.58 | 0.58 | | | | | |
| 0.57 | 3.56 | 0.55 | 41.0 | 116 | 3.12 | 2.96 | 0.22 |
| 0.56 | 3.45 | 0.54 | | | | | |
| 0.57 | 3.69 | 0.57 | | | | | |
| 0.57 | 3.57 | 0.55 | 39.6 | 114 | 3.14 | 2.82 | 0.22 |
| 0.55 | 3.51 | 0.54 | 41.4 | 118 | 3.19 | 2.87 | 0.22 |
| 0.56 | 3.60 | 0.57 | 39.7 | 113 | 3.09 | 2.83 | 0.23 |
| 0.58 | 3.67 | 0.57 | | | | | |
| 0.57 | 3.58 | 0.57 | 39.1 | 113 | 3.05 | 2.87 | 0.23 |
| 0.55 | 3.40 | 0.54 | 37.6 | 109 | 3.02 | 2.88 | 0.21 |
| 0.58 | 3.54 | 0.58 | 39.8 | 114 | 3.13 | 2.89 | 0.21 |
| 0.58 | 3.69 | 0.57 | | | | | |
| | | | | | | | |
| 0.56 | 3.57 | 0.56 | 39.8 | 114 | 3.03 | 2.65 | 0.21 |
| 0.57 | 3.74 | 0.59 | 40.2 | 114 | 2.97 | 3.00 | 0.21 |
| | | | | | | | |
| 0.61 | 3.91 | 0.61 | 42.2 | 119 | 2.98 | 3.13 | 0.51 |
| 0.63 | 3.84 | 0.62 | 44.3 | 127 | 3.10 | 3.21 | 0.20 |
| 0.66 | 4.13 | 0.65 | 44.8 | 128 | 3.09 | 3.17 | 0.20 |
| 0.57 | 3.49 | 0.56 | 39.6 | 113 | 2.94 | 2.75 | 0.19 |
| 0.65 | 4.12 | 0.66 | 44.9 | 127 | 3.13 | 3.37 | 0.22 |
| 0.03 | 0.20 | 0.03 | 2.00 | 5.30 | 0.07 | 0.18 | 0.01 |
| 28 | 28 | 28 | 20 | 20 | 20 | 20 | 19 |
| 2.43 | 7.64 | 4.80 | 23.6 | 2.77 | 0.03 | 2.80 | 0.26 |
| 1.95 | 1.95 | 1.95 | 2.06 | 2.25 | 2.32 | 2.45 | 2.40 |
| 0.02 | 0.18 | 0.03 | 1.96 | 4.24 | $<s_g$ | 0.15 | 0.01 |
| BIR | BIR | BIR | BHVO | W2 | W2 | W2 | W2 |
| | | | | | | | |
| 0.57 | 3.56 | 0.56 | 39.7 | 114 | 3.08 | 2.85 | 0.21 |
| 0.01 | 0.12 | 0.02 | 0.91 | 2.13 | 0.07 | 0.11 | 0.01 |
| 24 | 24 | 24 | 16 | 16 | 16 | 16 | 16 |
| | | | | | | | |
| 0.64 | 4.00 | 0.64 | 44.0 | 125 | 3.08 | 3.22 | 0.21 |
| 0.02 | 0.15 | 0.02 | 1.25 | 4.03 | 0.07 | 0.11 | 0.01 |
| 4 | 4 | 4 | 4 | 4 | 4 | 4 | 3 |
| 0.01 | 0.05 | 0.01 | 0.24 | 2.3 | 0.20 | 0.06 | 0.01 |

with a diversity of compositions. In the melt lens, localized convection prior to eruption results in partial homogenization of the liquids. The Leg 142 data is consistent with this model as evidenced by the convergence of the samples toward a predominantly homogeneous composition.

## Comparison of Parental Melt Compositions

From relative incompatible element abundances, the parental melt of Unit 1 may be more enriched than the parent of Unit 2 (see Fig. 7). The Unit 1 parent could simply be a smaller degree melt of the same source that yielded the parent of Unit 2 through more extensive melting. Alternatively, differences in trace element composition and the degree of depletion between melts can be created on a geologically short time scale, by repeated melt extractions from a single source. Assume the parental melt of Unit 1 was produced by a small degree of melting. The residual source would then be more depleted, and any further melt extracted from it, such as the parent of Unit 2, would reflect this depletion.

Unit 2 samples have generally lower MgO contents, suggesting that Unit 2 has experienced a greater extent of shallow fractional crystallization than Unit 1. This observation may provide an explanation for the fact that the concentrations of the REEs, Y, Zr, Hf and Ba, differ significantly between the units, yet Nb and Ta do not despite being highly incompatible elements. It is plausible that the Unit 1 pa-

rental melt (P1) has higher concentrations of highly incompatible elements, such as Nb, than the Unit 2 parental melt (P2). If so, P1 will have only slightly higher concentrations of moderately incompatible elements, such as Zr, than P2 (Fig. 7). The more extensive fractional crystallization experienced by Unit 2 samples will result in an increase in Unit 2 Nb and Ta concentrations to levels comparable to the Unit 1 samples. Because P1 and P2 have similar moderately incompatible element concentrations, however, fractionation crystallization will increase Zr and Y abundances in the Unit 2 samples to levels above those in Unit 1. The preceding relationships cannot be proven owing to the complex thermal histories of the samples, but are put forth as a possible explanation for the lack of variation in Nb and Ta concentrations. Alternatively, the absolute Nb and Ta contents in MORB may be too low relative to analytical error to detect subtle concentration variations.

## Temporal Relationship of Unit 1 and Unit 2

The fragmented nature of the Leg 142 recovery results in a dire lack of stratigraphic control regarding the relationship of Unit 1 to Unit 2. If the recovery depths are accepted without question, then Unit 2 lavas were emplaced before Unit 1, either as a separate eruptive event or as the first part of the same event. In this case, the melt feeding the magma chamber became on average slightly more enriched between the eruption of the Unit 2 and Unit 1 lavas, most likely a geologically short time interval because magma supply rate and eruption frequency are high along this segment of the East Pacific Rise. Alternatively, if recovery depth is ignored, variations between Units 1 and 2 represent heterogeneities within the same flow. In either case, the Leg 142 data set illustrates the degree of geochemical heterogeneity that can be expected at a single axial site. Lavas erupted at the ridge crest are the result of a continuous evolutionary process involving complex fractionation pathways and magma mixing; glass and whole rock compositions are averages of the entire process.

## Mantle Heterogeneity

It is well established that East Pacific Rise magmas are more isotopically homogeneous than Mid-Atlantic Ridge (MAR) magmas (e.g., Batiza, 1984; White et al., 1987; Harpp and White, 1990). Batiza (1984) argued that the isotopic homogeneity of EPR magmas results from mixing of isotopically heterogeneous magma batches in long-lived magma chambers. Long-lived or steady-state magma chambers are absent on the MAR; magmas are not homogenized before eruption. The isotopic homogeneity of the Leg 142 lavas, however, cannot be a result of homogenization within the axial magma chamber because these lavas exhibit compositional variations that must have existed before the parental melts entered the magma chamber. Mixing within the axial magma chamber has failed to obscure the elemental differences and would similarly have failed to obscure isotopic differences had they existed. The implication, therefore, is that the mantle beneath this segment of the EPR is inherently more isotopically homogeneous than that beneath the MAR. Differences in isotopic heterogeneity noted by Batiza (1984), among others, may therefore reflect differences between the Atlantic and Pacific suboceanic mantles rather than magma chamber processing. Large-scale processes such as mantle convection may be the major factors responsible for the degree of isotopic heterogeneity at mid-ocean ridges.

## SUMMARY AND CONCLUSIONS

Basalts collected from a single subsurface site at 9°30′N on the East Pacific Rise are homogeneous in terms of Sr, Nd and Pb isotopic ratios and Nb, Ta, Sr, Ni, Cu, and Zn concentrations, as well as most of their major oxide contents. The Leg 142 material falls into two dis-

**Table 5. Radiogenic isotope ratios determined by thermal ionization mass spectrometry, Site 864.**

| Core, section, interval (cm) | Sample type | Unit | $^{87}Sr/$ $^{86}Sr$ | $s_m$ | $^{143}Nd/$ $^{144}Nd$ | $s_m$ | $\varepsilon_{Nd}$ | $^{206}Pb/$ $^{204}Pb$ | $s_m$ | $^{207}Pb/$ $^{204}Pb$ | $s_m$ | $^{208}Pb/$ $^{204}Pb$ | $s_m$ |
|---|---|---|---|---|---|---|---|---|---|---|---|---|---|
| 142-864A- | | | | | | | | | | | | | |
| 1M-1, 0–10 | Powder | 1 | 0.702473 | 0.000006 | | | | 18.344 | 0.018 | 15.498 | 0.024 | 37.785 | 0.073 |
| 1M-2, 54–84 | Crystalline | 1 | 0.702495 | 0.000005 | 0.513142 | 0.000010 | 9.84 | 18.318 | 0.018 | 15.488 | 0.024 | 37.766 | 0.073 |
| 1M-2, 54–84 | Crystalline | 1 | 0.702472 | 0.000011 | 0.513113 | 0.000010 | 9.27 | | | | | | |
| 1M-2, 100–150 | Crystalline | 1 | 0.702488 | 0.000006 | 0.513124 | 0.000010 | 9.48 | 18.315 | 0.018 | 15.501 | 0.024 | 37.796 | 0.073 |
| 1M-2, 0–35 | Glass | 1 | 0.702477 | 0.000006 | 0.513143 | 0.000006 | 9.84 | 18.277 | 0.018 | 15.459 | 0.024 | 37.661 | 0.073 |
| 1M-2, 0–35 | Glass | 1 | | | | | | 18.312 | 0.018 | 15.484 | 0.024 | 37.722 | 0.073 |
| 1M-3, 0–35 | Glass | 1 | 0.702468 | 0.000011 | 0.513139 | 0.000010 | 9.77 | 18.296 | 0.018 | 15.467 | 0.024 | 37.660 | 0.073 |
| 1M-3, 0–35 | Glass | 1 | 0.702505 | 0.000007 | 0.513130 | 0.000010 | 9.60 | 18.285 | 0.018 | 15.445 | 0.024 | 37.588 | 0.073 |
| 1M-3, 0–35 | Glass | 1 | 0.702477 | 0.000007 | 0.513145 | 0.000007 | 9.88 | | | | | | |
| 1M-3, 55–85 | Powder | 1 | 0.702483 | 0.000006 | 0.513141 | 0.000005 | 9.82 | | | | | | |
| 1M-3, 54–84 | Crystalline | 1 | 0.702494 | 0.000005 | 0.513124 | 0.000010 | 9.48 | | | | | | |
| 1M-3, 54–84 | Crystalline | 1 | | | 0.513116 | 0.000010 | 9.33 | | | | | | |
| 1M-3, 100–150 | Powder | 1 | 0.702477 | 0.000007 | 0.513155 | 0.000007 | 10.08 | | | | | | |
| 1M-5, 0–100 | Powder | 1 | 0.702485 | 0.000007 | 0.513146 | 0.000006 | 9.92 | | | | | | |
| 1M-5, 0–100 | Glass* | 1 | 0.702473 | 0.000007 | 0.513110 | 0.000007 | 9.21 | 18.292 | 0.018 | 15.458 | 0.024 | 37.630 | 0.073 |
| 1M-5, 0–100 | Glass* | 1 | | | 0.513127 | 0.000010 | 9.54 | 18.293 | 0.018 | 15.470 | 0.024 | 37.692 | 0.073 |
| 1M-5, 0–100 | Crystalline | 1 | 0.702505 | 0.000007 | 0.513146 | 0.000010 | 9.91 | 18.355 | 0.018 | 15.490 | 0.024 | 37.755 | 0.073 |
| 1M-6, 0–75 | Glass | 1 | 0.702471 | 0.000007 | 0.513123 | 0.000010 | 9.46 | 18.327 | 0.018 | 15.502 | 0.024 | 37.809 | 0.073 |
| 1M-6, 0–75 | Glass | 1 | 0.702500 | 0.000006 | 0.513127 | 0.000010 | 9.54 | 18.312 | 0.018 | 15.483 | 0.024 | 37.717 | 0.073 |
| 1M-6, 0–75 | Glass | 1 | | | 0.513131 | 0.000007 | 9.61 | 18.290 | 0.018 | 15.464 | 0.024 | 37.678 | 0.073 |
| 1M-6, 0–75 | Powder | 1 | 0.702499 | 0.000011 | | | | | | | | | |
| 1M-6, 0–75 | Single glass | 1 | 0.702486 | 0.000007 | 0.513120 | 0.000007 | 9.41 | | | | | | |
| 1M-6, 0–75 | Single glass | 1 | 0.702489 | 0.000006 | 0.513124 | 0.000010 | 9.47 | | | | | | |
| 1M-6, 0–75 | Single glass | 1 | 0.702481 | 0.000007 | 0.513132 | 0.000010 | 9.63 | | | | | | |
| 1M-6, 0–75 | Single glass | 1 | 0.702472 | 0.000007 | 0.513140 | 0.000010 | 9.79 | | | | | | |
| 1M-6, 75–135 | Crystalline part | 1 | 0.702489 | 0.000005 | 0.513150 | 0.000010 | 9.98 | | | | | | |
| 1M-6, 75–135 | Glass part | 1 | 0.702477 | 0.000006 | | | | | | | | | |
| 142-864B- | | | | | | | | | | | | | |
| 2W-1, 0–4 | Crystalline | 1 | 0.702504 | 0.000007 | 0.513153 | 0.000010 | 10.05 | 18.310 | 0.018 | 15.491 | 0.024 | 37.759 | 0.073 |
| 2W-1, 0–4 | Crystalline | 1 | 0.702478 | 0.000011 | | | | | | | | | |
| 142-864A- | | | | | | | | | | | | | |
| 4Z-1, 9–15 | Crystalline | 2 | 0.702479 | 0.000005 | 0.513163 | 0.000010 | 10.24 | 18.268 | 0.018 | 15.467 | 0.024 | 37.644 | 0.073 |
| 4Z-1, 9–15 | Crystalline | 2 | 0.702490 | 0.000011 | 0.513151 | 0.000010 | 10.01 | 18.261 | 0.018 | 15.474 | 0.024 | 37.686 | 0.073 |
| 5Z-1, 5–9 | Crystalline | 2 | 0.702487 | 0.000005 | 0.513130 | 0.000010 | 9.59 | 18.275 | 0.018 | 15.465 | 0.024 | 37.664 | 0.073 |
| 5Z-1, 12–15 | Crystalline | 2(1) | 0.702482 | 0.000005 | 0.513126 | 0.000010 | 9.52 | 18.279 | 0.018 | 15.464 | 0.024 | 37.641 | 0.073 |
| 5Z-1, 12–15 | Crystalline | 2(1) | | | | | | 18.290 | 0.018 | 15.486 | 0.024 | 37.734 | 0.073 |
| 5Z-1, 24–30 | Powder | 2 | 0.702477 | 0.000005 | 0.513156 | 0.000005 | 10.10 | | | | | | |
| m | | | 0.702484 | | 0.513135 | | 9.70 | 18.300 | | 15.477 | | 37.705 | |
| $s_t$ | | | 0.000011 | | 0.000014 | | 0.27 | 0.025 | | 0.016 | | 0.062 | |
| $n$ | | | 30 | | 29 | | 29 | 19 | | 19 | | 19 | |
| $F_c$ | | | 1.03 | | 1.77 | | | 1.91 | | 0.46 | | 0.73 | |
| $F_{5\%}$ | | | 1.99 | | 2.08 | | | 2.10 | | 2.10 | | 2.10 | |

Note: $s_m$ = standard error of the mean for each sample ($s_a/n^{1/2}$, where x is the number of replicate analyses); * = small fragments; m = mean; $s_t$ = total standard deviation in the data set; $n$ = count; $F_c$, $F_{5\%}$, and 2(1) as in Table 4. During analysis, the $^{88}Sr$ ion beam intensity was maintained within 10% of $3 \times 10^{-11}$ A and 120 ratios were collected for each sample. Results were corrected for mass fractionation assuming a $^{86}Sr/^{88}Sr$ ratio of 0.1194 using an approximation of the exponential mass fractionation law. A $^{144}Nd$ ion beam intensity of $7.5 \times 10^{-12}$ A was maintained within 20% during the course of an analysis, and between 120 and 150 ratios were collected for each sample. Ratios were exponentially corrected for mass fractionation assuming a $^{146}Nd/^{144}Nd$ ratio of 0.721900. A $^{208}Pb$ aiming intensity of $2 \times 10^{-11}$ A was maintained within 25% during analysis. One hundred ratios were collected for every sample run. Data were corrected for fractionation based on the analysis of the NBS 981 Pb standard.

**Table 6. Results of F tests on Leg 142 Shipboard XRF data.**

| | $SiO_2$ | $TiO_2$ | $Al_2O_3$ | $Fe_2O_3$ | MnO | MgO | CaO | $Na_2O$ | $K_2O$ | $P_2O_5$ | Cr | Ni | V | Cu | Zn | Sr |
|---|---|---|---|---|---|---|---|---|---|---|---|---|---|---|---|---|
| m | 49.89 | 1.66 | 14.26 | 1.69 | 0.20 | 7.28 | 11.68 | 2.56 | 0.14 | 0.11 | 228 | 72 | 355 | 77 | 92 | 121 |
| $s_t$ | 0.14 | 0.05 | 0.13 | 0.19 | 0.01 | 0.13 | 0.11 | 0.05 | 0.02 | 0.01 | 19.2 | 4.1 | 10.4 | 11 | 6.1 | 1.9 |
| $n$ | 13 | 13 | 13 | 12 | 13 | 13 | 13 | 13 | 13 | 13 | 13 | 13 | 13 | 13 | 13 | 13 |
| $F_c$ | 1.61 | 27.7 | 2.05 | 90.7 | 0.42 | 1.14 | 13.7 | 0.42 | 5.60 | 1.31 | 367 | 4.2 | 6.8 | 129 | 37 | 3.4 |
| $F_{5\%}$ | 3.28 | 3.28 | 3.28 | 3.31 | 3.28 | 3.28 | 3.28 | 3.28 | 3.28 | 3.28 | 4.0 | 4.0 | 4.0 | 4.0 | 4.0 | 4.0 |

Note: Oxide concentrations in weight percent; others in ppm. m = mean; $s_t$ = total standard deviation in the data set; $n$ = count; $F_c$, $F_{5\%}$ as in Table 4. Analytical variances used in F test calculations are from the XRF standard report (Table 3) in the Leg 142 *Initial Reports* (Shipboard Scientific Party, 1993a).

**Table 7. ANOVA results.**

| | Ba | La | Ce | Pr | Nd | Sm | Eu | Gd | Tb | Dy | Ho | Er | Tm | Yb |
|---|---|---|---|---|---|---|---|---|---|---|---|---|---|---|
| ICP-MS data | | | | | | | | | | | | | | |
| Unit | 0.002 | 0.0001 | <0.0001 | <0.0001 | <0.0001 | <0.0001 | <0.0001 | <0.0001 | <0.0001 | <0.0001 | <0.0001 | <0.0001 | <0.0001 | <0.0001 |
| Sample type | 0.366 | 0.889 | 0.782 | 0.724 | 0.747 | 0.677 | 0.755 | 0.875 | 0.931 | 0.903 | 0.958 | 0.980 | 0.833 | 0.972 |

| | $TiO_2$ | $Fe_2O_3$ | CaO | $K_2O$ | Cr | Ni | V | Cu | Zn |
|---|---|---|---|---|---|---|---|---|---|
| Shipboard XRF data | | | | | | | | | |
| Unit | <0.0001 | 0.036 | <0.0001 | 0.981 | <0.0001 | 0.254 | 0.037 | 0.403 | 0.694 |

Note: Values represent probability that the differences within the data set when grouped by either unit or sample type (glassy vs. crystalline) could arise by chance. A value of 1 represents 100% certainty. n.a. = ANOVA test was not applied (see text for details).

tinct lithologic units based on the concentrations of several elements, including the REEs, Ba, Y, Zr, and Hf.

The relationship between Unit 1 and Unit 2 cannot be explained by shallow-level phenomena including fractional crystallization or crystal settling but must have originated below the magma chamber. This result is in agreement with other Leg 142 studies (Brophy and Allan, this volume; Brophy, this volume). Unit 1 and 2 samples are derived from two, or, more likely, a spectrum of similar but distinct parental melts. These parental melts shared the same mantle source, but evolved along different melt generation paths. As the melts migrated upward through the mush zone, they underwent a series of in situ fractionation processes. Liquids injected into the magma chamber have diverse compositions. In the melt lens, localized convection resulted in partial homogenization of the liquids and the observed convergence of the samples toward a single composition. This evolutionary melting process affected incompatible trace element concentrations more than the major and more compatible trace elements, a phenomenon reflected in the results of this study.

The precise temporal relationship between Units 1 and 2 cannot be determined because of the lack of stratigraphic control during drilling. Interunit geochemical variations may represent two (or more) eruptive events, or heterogeneity within a single flow. In either case, this information is useful in evaluating geochemical results from detailed axial studies, particularly from the immediate 9°–10°N ridge area.

The observation that at a single site on the EPR differences in trace element concentrations are accompanied by isotopic homogeneity suggests that geochemical characteristics of the underlying mantle, not shallow magma chamber processes, are the major factors controlling compositional variation at mid-ocean ridges. Large-scale phenomena such as mantle convection may be primarily responsible for the degree of isotopic heterogeneity at mid-ocean ridges, while complex mantle melting processes control trace element characteristics.

## ACKNOWLEDGMENTS

**Table 7 (continued).**

| Lu | Y | Zr | Nb | Hf | Ta |
|---|---|---|---|---|---|
| <0.0001 | <0.0001 | <0.0001 | n.a. | 0.002 | n.a. |
| 0.952 | 0.430 | 0.373 | n.a. | 0.330 | n.a. |

## REFERENCES*

Allègre, C.J., Hamelin, B., and Dupré, B., 1984. Statistical analysis of isotopic ratios of MORB: the mantle blob cluster model and the convective regime of the mantle. *Earth Planet. Sci. Lett.*, 71:71–84.

Batiza, R., 1984. Inverse relationship between Sr isotope diversity and rate of oceanic volcanism has implications for mantle heterogeneity. *Nature*, 309:440–441.

Batiza, R., and Niu, Y., 1992. Petrology and magma chamber processes at the East Pacific Rise ~9°30′N. *J. Geophys. Res.*, 97:6779–6797.

Cheatham, M.M., Sangrey, W.F., and White, W.M., 1993. Sources of error in external calibration ICP-MS analysis of geological samples and an improved non-linear drift correction procedure. *Spectrochim. Acta, Part B*, 48B:E487–E506.

Davis, J.C., 1986. *Statistics and Data Analysis in Geology* (2nd ed.): New York (Wiley).

Detrick, R.S., Buhl, P., Vera, E., Mutter, J., Orcutt, J., Madsen, J., and Brocher, T., 1987. Multi-channel seismic imaging of a crustal magma chamber along the East Pacific Rise. *Nature*, 326:35–41.

Hamelin, B., Dupré, B., and Allègre, C.J., 1984. Lead-strontium isotopic variations along the East Pacific Rise and the Mid-Atlantic Ridge: a comparative study. *Earth Planet. Sci. Lett.*, 67:340–350.

Harpp, K.S., 1994. Magmatic evolution of mid-ocean ridges and hotspots: Isotopic and trace element studies of the East Pacific Rise, Mid-Atlantic Ridge, and Galapagos Islands. [Ph.D. dissert.]. Cornell Univ., Ithaca, NY.

Harpp, K.S., and White, W.M., 1990. Isotopic study of contrasting magmatic systems: the East Pacific Rise at 9°–10°N and the MAR in the FAMOUS Area. *Eos*, 71:658.

Harpp, K.S., White, W.M., Batiza, R., and Castillo, P., 1991. Isotopic constraints on the East Pacific Rise magma chamber at 9°30′N. *Eos*, 72:496.

Hekinian, R., Thompson, G., and Bideau, D., 1989. Axial and off-axis heterogeneity of basaltic rocks from the East Pacific Rise at 12°35′N–12°51′N and 11°26′N–11°30′N. *J. Geophys. Res.*, 94:17437–17463.

Hurlbut, C.S., Jr., and Klein, C., 1977. *Manual of Mineralogy (after James D. Dana)* (19th ed.): New York (Wiley).

Jochum, K.P., Seufert, H.M., and Thirlwall, M.F., 1990. Multi-element analysis of 15 international standard rocks by isotope-dilution spark source mass spectrometry. *Geostand. Newsl.*, 14:469–473.

Kent, G.M., Harding, A.J., and Orcutt, J.A., 1990. Evidence for a smaller magma chamber beneath the East Pacific Rise at 9°30′N. *Nature*, 344:650–653.

Klein, E.M., and Langmuir, C.H., 1987. Ocean ridge basalt chemistry, axial depth, crustal thickness and temperature variations in the mantle. *J. Geophys. Res.*, 92:8089–8115.

Langmuir, C.H., Vocke, R.D., Jr., Hanson, G.N., and Hart, S.R., 1978. A general mixing equation with applications to Icelandic basalts. *Earth Planet. Sci. Lett.*, 37:380–392.

Longerich, H.P., 1993. Oxychlorine ions in inductively coupled plasma-mass spectrometry: effect of chlorine speciation as Cl⁻ and ClO₄⁻. *J. Anal. At. Spectrom.*, 8:439–444.

Macdougall, J.D., and Lugmair, G., 1986. Sr and Nd isotopes in basalts from the East Pacific Rise: significance for mantle heterogeneity. *Earth Planet. Sci. Lett.*, 77:273–284.

Miller, J.C., and Miller, J.N., 1992. *Statistics for Analytical Chemistry*: West Sussex, England (Ellis Horwood).

Nakamura, N., Yamamoto, K., Noda, S., Nishikawa, Y., Komi, H., Nagamoto, H., Nakayama, T., and Misawa, K., 1989. Determination of picogram quantities of rare-earth elements in meteoritic materials by direct-loading thermal ionization mass spectrometry. *Anal. Chem.*, 61:755–762.

Nielsen, R.L., 1985. EQUIL.FOR: a program for the modeling of low-pressure differentiation processes in natural mafic magma bodies. *Comput. Geosci.*, 11:531–546.

————, 1988. A model for the simulation of combined major and trace element liquid lines of descent. *Geochim. Cosmochim. Acta*, 52:27–38.

*Abbreviations for names of organizations and publications in ODP reference lists follow the style given in *Chemical Abstracts Service Source Index* (published by American Chemical Society).

Nielsen, R.L., and Dungan, M.E., 1983. Low-pressure mineral-melt equilibria in natural anhydrous mafic systems. *Contrib. Mineral. Petrol.,* 84:310–326.

Nielsen, R.L., Gallahan, W.E., and Newberger, F., 1992. Experimentally determined mineral-melt partition coefficients for Sc, Y and REE for olivine, orthopyroxene, pigeonite, magnetite and ilmenite. *Contrib. Mineral. Petrol.,* 110:488–499.

Prinzhofer, A., Lewin, E., and Allègre, C.J., 1989. Stochastic melting of the marble cake mantle: evidence from local study of the East Pacific Rise at 12°50'N. *Earth Planet. Sci. Lett.,* 92:189–206.

Shaw, D.M., and Cruft, E.F., 1967. Homogeneity and random events in geochemistry. *In* Vinogradov, A.P. (Ed.), *Chemistry of the Earth's Crust* (Vol. 2). Acad. Sci. USSR, V.I. Vernadskii Inst. Geochem. Anal. Chem., 301–314.

Shipboard Engineering and Scientific Parties, 1993. Introduction, background, and scientific objectives: engineering Leg 142 at the East Pacific Rise. *In* Storms, M.A., Batiza, R., et al., *Proc. ODP, Init. Repts.,* 142: College Station, TX (Ocean Drilling Program), 31–40.

Shipboard Scientific Party, 1993a. Explanatory notes. *In* Storms, M.A., Batiza, R., et al., *Proc. ODP, Init. Repts.,* 142: College Station, TX (Ocean Drilling Program), 41–52.

—————, 1993b. Site 864. *In* Storms, M.A., Batiza, R., et al., *Proc. ODP, Init. Repts.,* 142: College Station, TX (Ocean Drilling Program), 55–72.

Sinton, J.M., and Detrick, R.S., 1992. Mid-ocean ridge magma chambers. *J. Geophys. Res.,* 97:197–216.

Sinton, J.M., Smaglik, S.M., and Mahoney, J.J., 1991. Magmatic processes at superfast spreading mid-ocean ridges: glass compositional variations along the East Pacific Rise 13°–23°S. *J. Geophys. Res.,* 96:6133–6155.

Snedecor, G.W., and Cochran, W.G., 1989. *Statistical Methods:* Ames, IA (Iowa State Univ. Press).

Toomey, D.R., Purdy, G.M., Solomon, S.C., and Wilcock, W.S.D., 1990. The three-dimensional seismic velocity structure of the East Pacific Rise near latitude 9°30'N. *Nature,* 347:639–645.

Verma, S.P., 1992. Seawater alteration effects on REE, K, Rb, Cs, Sr, U, Th, Pb and Sr-Nd-Pb isotope systematics of mid-ocean ridge basalt. *Geochem. J.,* 26:159–177.

White, W.M., and Dupré, B., 1986. Sediment subduction and magma genesis in the Lesser Antilles: isotopic and trace element constraints. *J. Geophys. Res.,* 91:5927–5941.

White, W.M., Hofmann, A.W., and Puchelt, H., 1987. Isotope geochemistry of Pacific mid-ocean ridge basalt. *J. Geophys. Res.,* 92:4881–4893.

White, W.M., and Patchett, J., 1984. Hf-Nd-Sr isotopes and incompatible element abundances in island arcs: implications for magma origins and crust-mantle evolution. *Earth Planet. Sci. Lett.,* 67:167–185.